Cell Reports

Article

Generation of Lungs by Blastocyst Complementation in Apneumic Fgf10-Deficient Mice

Graphical Abstract

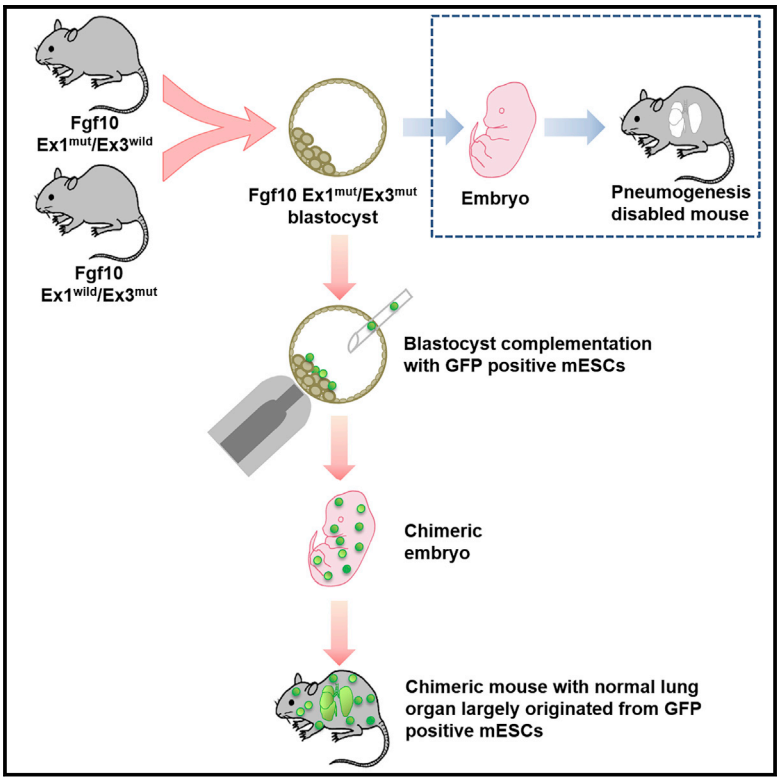

Highlights

- Lungs are generated in apneumic *Fgf10*-deficient mice by blastocyst complementation
- Complementation with mouse ESCs enables *Fgf10*-deficient mice to survive to adulthood
- The generated lung alveolar parenchyma largely originate from the injected mouse ESCs
- The interstitial portions of the lung also largely originate from the injected mouse ESCs

Authors

Akihiko Kitahara, Qingsong Ran, Kanako Oda, ..., Yoichi Ajioka, Yasuo Saijo, Qiliang Zhou

Correspondence

yasosj@med.niigata-u.ac.jp (Y.S.), zhouql@med.niigata-u.ac.jp (Q.Z.)

In Brief

Kitahara et al. generate lungs from mouse embryonic stem cells (ESCs) in apneumic *Fgf10* Ex1^{mut}/Ex3^{mut} mice by blastocyst complementation. Complementation with ESCs enables *Fgf10*-deficient mice to survive to adulthood without abnormalities. The generated lungs in *Fgf10* Ex1^{mut}/Ex3^{mut} mice are composed largely of the injected ESC-derived cells.

Kitahara et al., 2020, Cell Reports *31*, 107626
May 12, 2020
https://doi.org/10.1016/j.celrep.2020.107626

CellPress

Cell Reports

CellPress
OPEN ACCESS

Article

Generation of Lungs by Blastocyst Complementation in Apneumic Fgf10-Deficient Mice

Akihiko Kitahara,[1,5,8] Qingsong Ran,[1,8] Kanako Oda,[2] Akihiro Yasue,[3] Manabu Abe,[4] Xulu Ye,[1] Toshikuni Sasaoka,[2] Masanori Tsuchida,[5] Kenji Sakimura,[6] Yoichi Ajioka,[7] Yasuo Saijo,[1,*] and Qiliang Zhou[1,9,*]

[1]Department of Medical Oncology, Niigata University Graduate School of Medical and Dental Sciences, 1-757 Asahimachi-dori Chuo-ku, Niigata 951-8510, Japan

[2]Department of Comparative and Experimental Medicine, Brain Research Institute, Niigata University, 1-757 Asahimachi-dori, Chuo-ku, Niigata 951-8585, Japan

[3]Department of Orthodontics and Dentofacial Orthopedics, Institute of Biomedical Sciences, Tokushima University Graduate School, 3-18-15 Kuramoto-cho, Tokushima 770-8504, Japan

[4]Department of Cellular Neurobiology, Brain Research Institute, Niigata University, 1-757 Asahimachi-dori, Chuo-ku, Niigata 951-8585, Japan

[5]Division of Thoracic and Cardiovascular Surgery, Niigata University Graduate School of Medical and Dental Sciences, 1-757 Asahimachi-dori Chuo-ku, Niigata 951-8510, Japan

[6]Department of Animal Model Development, Brain Research Institute, Niigata University, 1-757 Asahimachi-dori, Chuo-ku, Niigata 951-8585, Japan

[7]Division of Molecular and Diagnostic Pathology, Niigata University Graduate School of Medical and Dental Sciences, 1-757 Asahimachi-dori Chuo-ku, Niigata 951-8510, Japan

[8]These authors contributed equally

[9]Lead Contact

*Correspondence: yasosj@med.niigata-u.ac.jp (Y.S.), zhouql@med.niigata-u.ac.jp (Q.Z.)

https://doi.org/10.1016/j.celrep.2020.107626

SUMMARY

The shortage of donor lungs hinders lung transplantation, the only definitive option for patients with end-stage lung disease. Blastocyst complementation enables the generation of transplantable organs from pluripotent stem cells (PSCs) in animal models. Pancreases and kidneys have been generated from PSCs by blastocyst complementation in rodent models. Here, we report the generation of lungs using mouse embryonic stem cells (ESCs) in apneumic *Fgf10* Ex1^{mut}/Ex3^{mut} mice by blastocyst complementation. Complementation with ESCs enables *Fgf10*-deficient mice to survive to adulthood without abnormalities. Both the generated lung alveolar parenchyma and the interstitial portions, including vascular endothelial cells, vascular and parabronchial smooth muscle cells, and connective tissue, largely originate from the injected ESCs. These data suggest that *Fgf10* Ex1^{mut}/Ex3^{mut} blastocysts provide an organ niche for lung generation and that blastocyst complementation could be a viable approach for generating whole lungs.

INTRODUCTION

Lung transplantation is the only definitive option for patients with end-stage lung disease and is performed worldwide with steadily improving outcomes. However, a critical shortage of donor lungs and graft rejection are issues that need to be overcome. Bioengineered lungs created by recellularizing an acellular whole-lung scaffold with endothelial and epithelial cells by using a bioreactor transplanted orthotopically in animal models have exhibited temporary gas exchange (Petersen et al., 2010; Ott et al., 2010; Song et al., 2011; Nichols et al., 2018). Lungs have also been generated from human-induced pluripotent stem cell (PSC)-derived epithelial cells on native extracellular matrices (Ghaedi et al., 2018). However, the generation of normally functioning lungs *in vitro* is considered impractical because it remains difficult to replicate organogenesis *in vitro* by adequately recellularizing the lung scaffold with appropriately differentiated stem cells (to repopulate the various lung cell phenotypes in their usual anatomic sites) (Farré et al., 2018; Meyer, 2018).

Blastocyst complementation shows promise for organ generation. Recipient blastocysts derived from mutant animals with deficiencies in particular organs could provide organ niches for developmental compensation by wild-type PSCs (Kobayashi et al., 2010; Rashid et al., 2014; Yamaguchi et al., 2017; Usui et al., 2012; Freedman, 2018; Goto et al., 2019). Indeed, the generation of PSC-derived pancreases in apancreatic Pdx1$^{mut/mut}$ rodents by blastocyst complementation in an intra- or interspecies setting was reported by Kobayashi et al., 2010; Yamaguchi et al., 2017. The generated pancreases were composed almost entirely of injected donor PSCs, with the exception of structures not influenced by *Pdx1* expression, such as vessels, nerves, and some interstitial cells (Kobayashi et al., 2010; Yamaguchi et al., 2017). Interestingly, when transplanted into mice with diabetes,

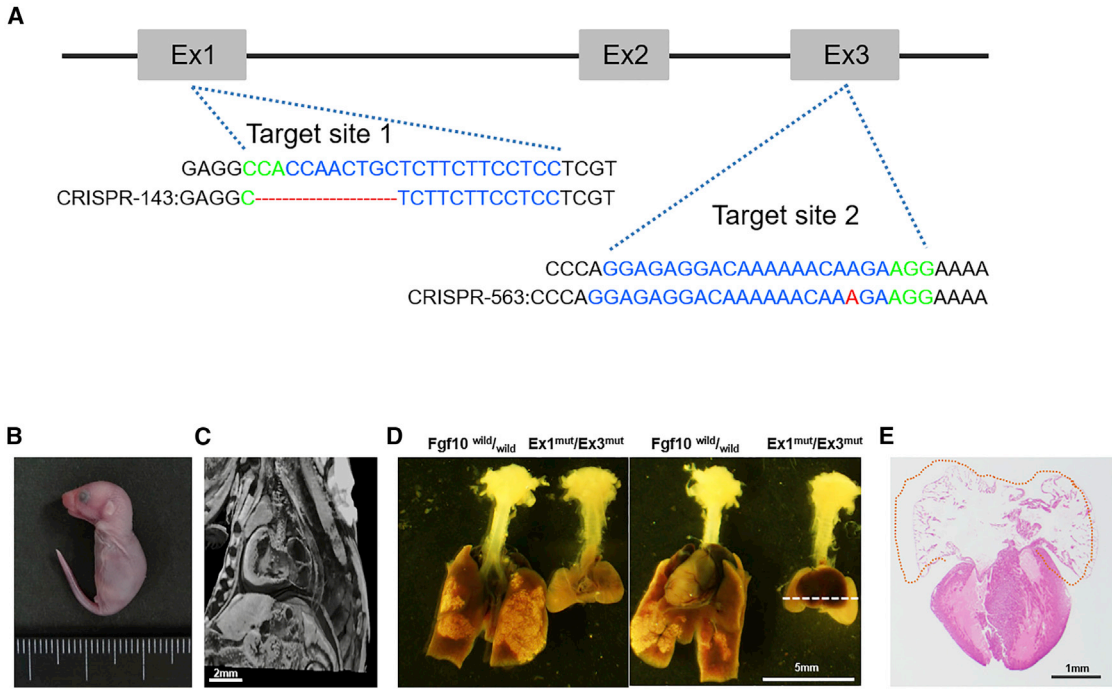

Figure 1. Generation of *Fgf10*-Knockout Mice

(A) Schematic representation of target sites in *Fgf10* by using the CRISPR-Cas9 system and mutations in the founder mouse. Protospacer and protospacer adjacent motif (PAM) sequences are shown in blue and green text, respectively. The CRISPR-143 founder mouse had a 10-base deletion in *Fgf10* Ex1 (red dashes) and the CRISPR-563 founder mouse had a 1-base insertion in *Fgf10* Ex3 (red letter).

(B) *Fgf10* Ex1^{mut}/Ex3^{mut} neonate. (C) Sagittal micro-CT image of the *Fgf10* Ex1^{mut}/Ex3^{mut} neonate. Scale bar, 2 mm. See also the continuous micro-CT images in Videos 1 and 2 online.

(D) Macroscopic images of the tracheas, lungs, and hearts of *Fgf10* $^{wild/wild}$ and Ex1^{mut}/Ex3^{mut} neonates. Left and right, back and front views, respectively. Scale bar, 5 mm.

(E) H&E staining of the tissue section indicated by the white dotted line in the right panel of (D). The orange dotted line demarcates an atrium with a large atrial appendage without lung tissue. Scale bar, 1 mm.

islets derived from mouse PSCs by interspecies blastocyst complementation normalized the host blood glucose level for over 1 year without continuous immunosuppression (Yamaguchi et al., 2017). Similarly, mouse PSC-derived generation of kidneys was successful in anephric Sall1$^{mut/mut}$ models in allogenic (Usui et al., 2012; Freedman, 2018) and interspecific (Goto et al., 2019) settings.

Fibroblast growth factor 10 (Fgf10), a mesenchymal-epithelial signaling molecule, is the key regulator of lung development. *Fgf10* is initially expressed in the splanchnic mesenchyme surrounding the ventral foregut mesoderm at embryonic day 9.5 (E9.5), when the primary lung buds start to emerge, and is subsequently restricted to the distal lung mesenchyme at sites where branching occurs from E10.5 to E12.5 in mice (Bellusci et al., 1997; Yuan et al., 2018). Fgf10 is essential for regulating epithelial proliferation and lung branching morphogenesis (Yuan et al., 2018; Sekine et al., 1999). Intriguingly, in the embryonic lung, Fgf10 directly and indirectly orchestrates the differentiation of mesenchymal progenitors into multiple lineages, including endothelium, parabronchial and vascular smooth muscle cells, lipofibroblasts (LIFs), interstitial fibroblasts, alveolar myofibroblasts, and nerve cells (Yuan et al., 2018; El Agha and Bellusci, 2014; Chao et al., 2015; El Agha et al., 2014; Chao et al., 2019). The absence of Fgf10 or its receptor Fgfr2b in mice results in lung deficiency, causing perinatal lethality, as well as in limb and thyroid agenesis (Sekine et al., 1999; De Moerlooze et al., 2000; Ohuchi et al., 2000). Therefore, Fgf10 deficiency may provide an ideal "organ niche" for generating lungs from PSCs by blastocyst complementation.

Here, we report the generation of lungs from mouse embryonic stem cells (ESCs) in apneumic Fgf10 Ex1^{mut}/Ex3^{mut} mice by blastocyst complementation. Complementation with ESCs enabled Fgf10-deficient mice to survive to adulthood without abnormalities. The generated lungs (including not only the lung parenchyma but also the blood vessels and connective tissues) in *Fgf10* Ex1^{mut}/Ex3^{mut} mice were composed largely of the injected ESC-derived cells.

RESULTS

Generation and Characterization of Fgf10-Knockout Mice

We first created *Fgf10*-knockout mice to provide the necessary developmental niche for lung generation. As shown in Figure 1, we developed *Fgf10* Ex1$^{-/-}$ mice and *Fgf10* Ex3$^{-/-}$ mice (CRISPR-143: 10-base deletions in Ex1 and

CRISPR-563: 1-base insertion in Ex3, respectively) (Yasue et al., 2014) by microinjecting the clustered regularly interspaced short palindromic repeats (CRISPR)-Cas9 constructs into the cytoplasm of mouse zygotes. Both *Fgf10* Ex1$^{-/-}$ and *Fgf10* Ex3$^{-/-}$ mice exhibited limb and lung deficiencies, as did *Fgf10*-knockout mice (Sekine et al., 1999; Yasue et al., 2014). Although the *Fgf10* Ex1$^{-/-}$ or *Fgf10* Ex3$^{-/-}$ mice can provide the necessary developmental niche for generating lungs from wild-type ESCs, genotyping of the ESC-derived chimeric mice would be difficult because wild-type DNA would be mixed in their bodies during the injection of wild-type ESCs. In previous studies, sorting of recipient cells and a single-recipient hematopoietic-stem-cell-derived colony analysis were performed to identify the genotype of host mice (Kobayashi et al., 2010; Yamaguchi et al., 2017; Usui et al., 2012; Goto et al., 2019); however, these methods are time-consuming and the results can be inconclusive. We investigated the feasibility of using compound heterozygous mutant (*Fgf10* Ex1^{mut}/Ex3^{mut}) embryos for ESCs injection to facilitate genotyping. We intercrossed *Fgf10* Ex1$^{-/+}$ founder mice (CRISPR-143 line) with *Fgf10* Ex3$^{-/+}$ founder mice (CRISPR-563 line) by *in vitro* fertilization and obtained 64 blastocysts. Those blastocysts were transferred into the uteri of pseudopregnant mice, and 19 neonates were obtained (Table S1). Four neonates exhibited limb deficiencies (Figure 1B) and died at birth. Genotyping revealed that these limb-deficient neonates were derived from *Fgf10* Ex1^{mut}/Ex3^{mut} embryos (Figure S1). Despite the small population, *Fgf10* $^{wild/wild}$, *Fgf10* Ex1^{mut}/Ex3^{wild}, *Fgf10* Ex1^{wild}/Ex3^{mut}, and *Fgf10* Ex1^{mut}/Ex3^{mut} mice were born at an almost-Mendelian ratio (Table S1). Gross anatomy, hematoxylin and eosin (H&E) staining, and microcomputed tomography (micro-CT) analyses confirmed that all *Fgf10* Ex1^{mut}/Ex3^{mut} neonates exhibited lung deficiency (Figures 1C–1E and 2; Video S1) or severe lung hypoplasia (Video S2). Thus, we used the *Fgf10* Ex1^{mut}/Ex3^{mut} compound heterozygous mutant mice for lung generation by blastocyst complementation in subsequent experiments.

Generation of Lungs in Apneumic Fgf10 Ex1^{mut}/Ex3^{mut} Mice

We next generated lungs by using wild-type green fluorescent protein (GFP)-positive mouse ESCs by blastocyst complementation in apneumic *Fgf10* Ex1^{mut}/Ex3^{mut} mice. A total of 121 blastocysts microinjected with ESCs was transferred into pseudopregnant mouse uteri, and 43 neonates (36%) were obtained. Genotyping revealed that *Fgf10* $^{wild/wild}$, *Fgf10* Ex1^{mut}/Ex3^{wild}, *Fgf10* Ex1^{wild}/Ex3^{mut}, and *Fgf10* Ex1^{mut}/Ex3^{mut} neonates were born at a Mendelian ratio (Table S2). A total of 20 of 43 neonates (47%) was identified as chimeras by confirming GFP expression. All of the chimeras exhibited a normal phenotype without limb deficiencies. Genotyping revealed that 5 of 20 chimeras (40%) were derived from *Fgf10* Ex1^{mut}/Ex3^{mut} embryos (Tables 1 and S2). The *Fgf10* Ex1^{mut}/Ex3^{mut} chimeras exhibited a significant body-weight gain compared with *Fgf10* wild-type and *Fgf10* Ex1^{mut}/Ex3^{mut} mice, whereas no significant difference was observed between the groups of chimeric neonates (Figure S2B), which is consistent with previous observations (Lan et al., 2016; Mori et al., 2019). Macroscopic analysis and micro-CT confirmed the existence of a lung in the thoracic cavity of the *Fgf10* Ex1^{mut}/Ex3^{mut} chimeras (Figures 2A and 2D; continuous CT images in Video 3). The lungs of the *Fgf10* Ex1^{mut}/Ex3^{mut} chimeras were grossly and histologically normal (Figures 2B, 2C, and S2A). *Fgf10* Ex1^{mut}/Ex3^{mut} chimeras, as well as Ex1^{mut}/Ex3^{wild} chimeras, exhibited extremely strong GFP expression, indicating the contribution of GFP-expressing ESCs in various organs (Figure 2A). Although GFP expression in the lung was weaker than that in skin and limb tissues in chimeras (Figure 2A), the lung expressed GFP to a greater degree than negative controls (Figure 2B). However, it was difficult to distinguish the GFP expression level between *Fgf10* Ex1^{mut}/Ex3^{mut} and Ex1^{mut}/Ex3^{wild} chimeras at the neonate stage by using either in macroscopic or microscopic analysis (Figure 2B). Nevertheless, these results indicated that lungs were generated in apneumic *Fgf10* Ex1^{mut}/Ex3^{mut} mice by blastocyst complementation.

Complementation with Mouse ESCs Rescues the Fgf10 Ex1^{mut}/Ex3^{mut} Mice

Next, we investigated whether the *Fgf10* Ex1^{mut}/Ex3^{mut} chimeric mice could survive to adulthood. A total of 638 microinjected embryos was transferred into pseudopregnant mouse uteri, and 153 neonates (24%) were obtained (Tables 1 and S3). Confirming GFP expression identified 76 neonates (50%) as chimeras, but 36 of them died at birth, whereas 16 of 40 live chimera neonates survived until weaning. Notably, 5 of 16 weaned chimeric mice were confirmed to be derived from compound heterozygous embryos (*Fgf10* Ex1^{mut}/Ex3^{mut}) by genomic analysis using the Surveyor system and DNA sequencing (Figure S2). These five *Fgf10* Ex1^{mut}/Ex3^{mut} chimeric mice survived well without any abnormalities in appearance, compared with *Fgf10* $^{wild/wild}$ mice. No respiratory symptoms, such as dyspnea or wheezes, were observed in these compound heterozygous chimeric mice. For histological analysis, *Fgf10* Ex1^{mut}/Ex3^{mut} chimeric mice were sacrificed 4 months after birth. As reported previously (Kobayashi et al., 2010; Usui et al., 2012; Goto et al., 2019), the mouse ESCs contributed to all of the tissues, including germ cells, to various degrees and among individuals depending on the degree of chimerism, as indicated by the different expression levels of GFP (Figures 3A, 4, 5, S4, and S6). *Fgf10* Ex1^{mut}/Ex3^{mut} chimeric adult mouse no. 2 exhibited lower amplification of the frameshift mutation sequence than other *Fgf10* Ex1^{mut}/Ex3^{mut} chimeric adult mice, such as no. 1, indicating that chimerism in mouse no. 2 was relatively high (Figure S3C). Furthermore, in mouse no. 2, DNA samples from lung tissues exhibited a low density of cleaved bands and low amplification of the frameshift mutation sequence, indicating that ESCs contributed substantially to the lung tissues (Figures S4C and S5). This finding was validated by immunofluorescence staining. In contrast to the low level of GFP expression in other tissues (Figure S6), strong GFP expression was observed in almost all the lung tissue (Figures 3A, 4, and 5). These data demonstrated that organ deficiencies in *Fgf10* Ex1^{mut}/Ex3^{mut} mice could be rescued by ESCs by blastocyst complementation, implying that it is feasible to use ESCs to generate lungs in *Fgf10* Ex1^{mut}/Ex3^{mut} mice.

Characterization of Lungs in Adult Fgf10 Ex1^{mut}/Ex3^{mut} Chimeric Mice

No significant morphological changes were observed in the lungs of Fgf10 Ex1^{mut}/Ex3^{mut} adult chimeras, compared with

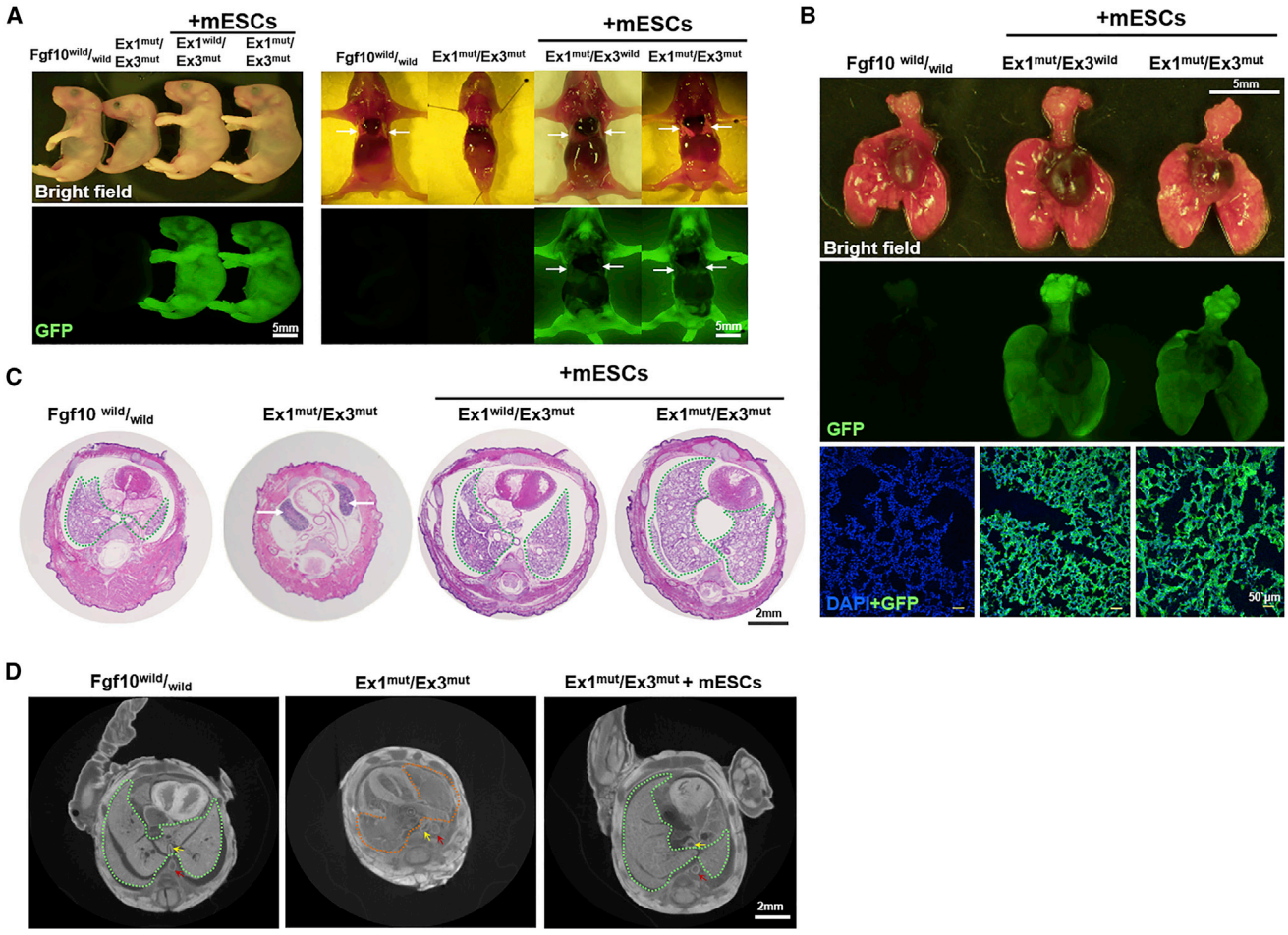

Figure 2. Generation of Mouse ESC-Derived Lung in *Fgf10* Ex1^{mut}/Ex3^{mut} Mice by Blastocyst Complementation (Analysis at the Neonatal Stage)

(A) Macroscopic phenotypes of *Fgf10* Ex1^{wild}/Ex3^{mut} and Ex1^{mut}/Ex3^{mut} chimeric neonates compared with *Fgf10* $^{wild/wild}$ and Ex1^{mut}/Ex3^{mut} neonates as controls. Left, macroscopic appearance; right, macroscopic views after thoracotomy and laparotomy. White arrows indicate lung tissues. Top, bright-field images; bottom, fluorescence images. Scale bars, 5 mm.

(B) The tracheas, lungs, and hearts extracted from control *Fgf10* $^{wild/wild}$, Ex1^{mut}/Ex3^{wild}, and Ex1^{mut}/Ex3^{mut} chimeric neonates. GFP expression in macro tissues and frozen micro sections are shown in the middle and bottom panels, respectively. Scale bars, 5 mm in macro images and 50 μm for frozen sections.

(C) H&E staining of thoracic cross-sections of the *Fgf10* $^{wild/wild}$ and Ex1^{mut}/Ex3^{mut} neonates and the *Fgf10* Ex1^{mut}/Ex3^{mut} and Ex1^{wild}/Ex3^{mut} chimeric neonates. Scale bar, 2 mm. The green dotted line indicates the lung. White arrows indicate the thymus.

(D) Axial micro-CT image of *Fgf10* $^{wild/wild}$ and Ex1^{mut}/Ex3^{mut} neonates, and the *Fgf10* Ex1^{mut}/Ex3^{mut} chimeric neonate. Scale bar, 2 mm. See also the continuous micro-CT images in Videos 1, 2, and 3 online. The orange dotted line demarcates an atrium with a large atrial appendage in an *Fgf10* Ex1^{mut}/Ex3^{mut} mouse. Green dotted lines indicate the lung. Yellow and red arrows indicate the esophagus and the thoracic aorta, respectively.

adult Fgf10 $^{wild/wild}$ mice or Fgf10 Ex1^{wild}/Ex3^{mut} chimeras (Figure 3A). GFP was expressed in a diffuse manner across the entire lung in Fgf10 Ex1^{mut}/Ex3^{mut} adult chimeras, and the expression level was considerably stronger than that in cardiac tissue of the same mouse or lung tissue of adult Fgf10 Ex1^{wild}/Ex3^{mut} chimeric mice (Figure 3A). Lung tissues in adult Fgf10 Ex1^{mut}/Ex3^{mut} chimeric mice were histologically normal compared with those of adult Fgf10 $^{wild/wild}$ mice (Figures 3B

Table 1. Results of Blastocyst Complementation for Lung Generation

Analysis Stage	No. of Blastocyst Transferred	No. (%) of Neonates	No. (%) of Chimeric Fetuses	No. (%) of Chimeras Weaned	No. by Genotype			No. (%) of Lung Complemented
					Wild/Wild	Ex1 or Ex3 Hetero	Compound Hetero	
Neonate	121	43 (36)	20 (47)		13	2	5	5 (100)
Adult	638	153 (24)	76 (50)	16 (21)	6	5	5	5 (100)

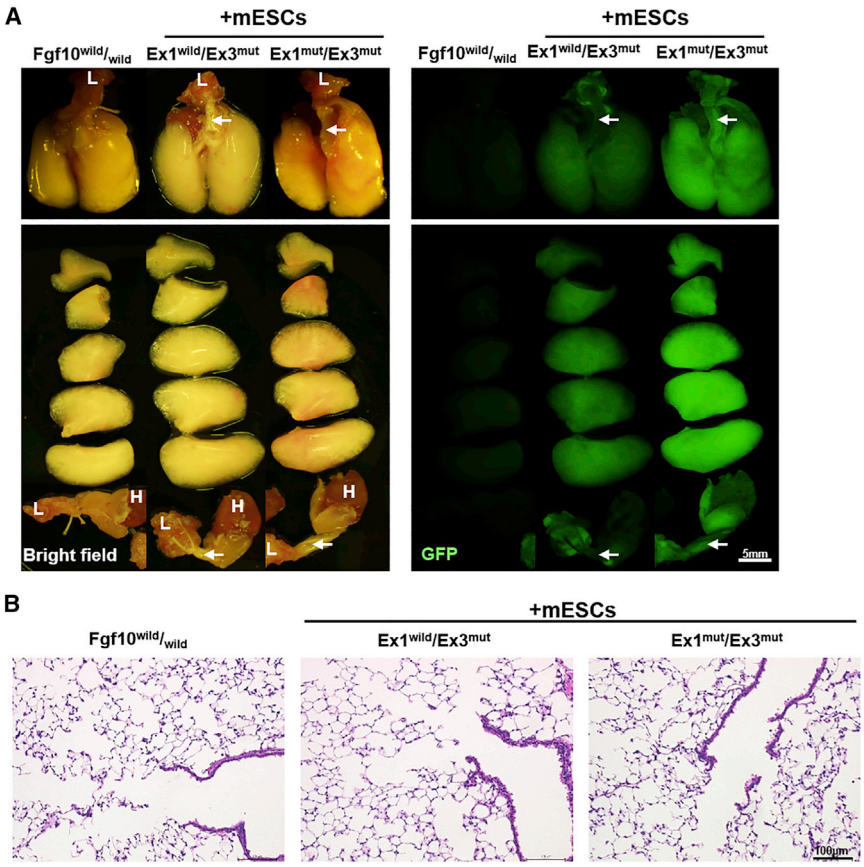

Figure 3. The Generation of a Mouse ESC-Derived Lung in *Fgf10* Ex1^{mut}/Ex3^{mut} Mice by Blastocyst Complementation (Analysis at the Adult Stage)

(A and B) Bright-field and GFP-fluorescence images of the lung (A) and H&E-stained images of lung tissues from adult *Fgf10* $^{wild}/_{wild}$ mice and Ex1^{wild}/Ex3^{mut} and Ex1^{mut}/Ex3^{mut} chimeric mice (B). The blood in lung tissues was washed out by infusing physiological saline into the right ventricle before extraction. H, heart; L, larynx. White arrows indicate the trachea. Scale bar, 5 mm for (A) and 100 μm for (B).

and S4A). Parenchymal and interstitial cells in the lung of adult Fgf10 Ex1^{mut}/Ex3^{mut} chimeric mice exhibited strong GFP fluorescence (Figures 4 and 5). As shown in Figure 4, most of the T1α-positive type I alveolar cells and surfactant protein C (SPC)-positive type II alveolar cells were GFP positive, indicating that these cells were mainly derived from ESCs. In Fgf10 Ex1^{mut}/Ex3^{mut} chimeric adult mouse no. 2, almost the entire population of SPC-positive cells (93.84% ± 4.46%) (Data are presented as the means ± standard deviation.) and the majority of Clara cell secretory protein (CCSP)-positive club cells (77% ± 15.82%) in respiratory and terminal bronchioles were GFP positive (Figure 4C). Notably, most of the CCSP-negative epithelial cells (nonclub cells) in terminal bronchioles also expressed GFP (Figure 4C). In addition, ciliated cells in bronchioles were GFP positive (Figure S4D). The percentage of GFP-positive club cells in the primary and lobe bronchi was relatively low (65.05% ± 18.51%). In Fgf10 Ex1^{mut}/Ex3^{mut} chimeric adult mouse no. 1, the percentages of SPC-positive cells and CCSP-positive club cells in respiratory and terminal bronchioles expressing GFP were relatively low (80.65% ± 9.72% and 72.2% ± 13.48%, respectively). The expression pattern of thyroid transcription factor 1 (TTF-1), a member of the homeodomain transcription factor family, in adult Fgf10 Ex1^{mut}/Ex3^{mut} chimeric mice was identical to that in Fgf10 $^{wild/wild}$ mice. Most of the TTF-1-positive cells were confirmed to be GFP-positive (Figure 4A). Furthermore, most of the CD31-positive cells strongly expressed GFP (Figure 5A), indicating that the vascular endothelial cells were derived from ESCs. In the same manner, large portions of the α-smooth muscle actin (α-SMA)- and vimentin-positive cells (Figures 5B–5D) were GFP positive, indicating that the vascular and parabronchial smooth muscle cells, connective tissues surrounding the blood vessels and airway, and visceral pleura were largely formed from the ESCs. βIII-Tubulin-positive nerve cells were the exception to this (Figure S4D). In contrast, only a small portion of the various lung tissues of adult Fgf10 Ex1^{wild}/Ex3^{mut} chimeric mice exhibited expression of GFP (Figures 4 and 5). These data indicated that the majority of the lungs was generated from mouse ESCs in adult Fgf10 Ex1^{mut}/Ex3^{mut} chimeric mice by blastocyst complementation and matured normally.

DISCUSSION

We generated lung organs in apneumic Fgf10 Ex1^{mut}/Ex3^{mut} mice by blastocyst complementation using mouse ESCs. Some of these chimeric mice grew to adulthood with normal phenotypes, although the efficacy of blastocyst complementation was low. The generated lungs were morphologically normal. The cells in the generated lungs were a mixture of recipient cells and GFP-positive ESCs.

Lung deficiency has been reported in several knockout mouse models, as a result of disrupting molecules essential for lung development. Knockout of *Fgf10* caused lung agenesis, whereas trachea formation remained (Sekine et al., 1999). The absence of fibroblast growth factor receptor 2b (Fgfr2b), the main Fgf10 receptor expressed in the epithelia of the developing lung, results in lung, but not trachea, deficiency (De Moerlooze et al., 2000; Ohuchi et al., 2000). Inactivation of Wnt/β-catenin signaling by knockout of *Ctnnb1*, which encodes β-catenin expressed in the endoderm, results in a defect in the initial specification of the primary lung and a complete absence of lung and trachea development (Harris-Johnson et al., 2009; Goss et al., 2009). These knockout mouse models of lung deficiency provide

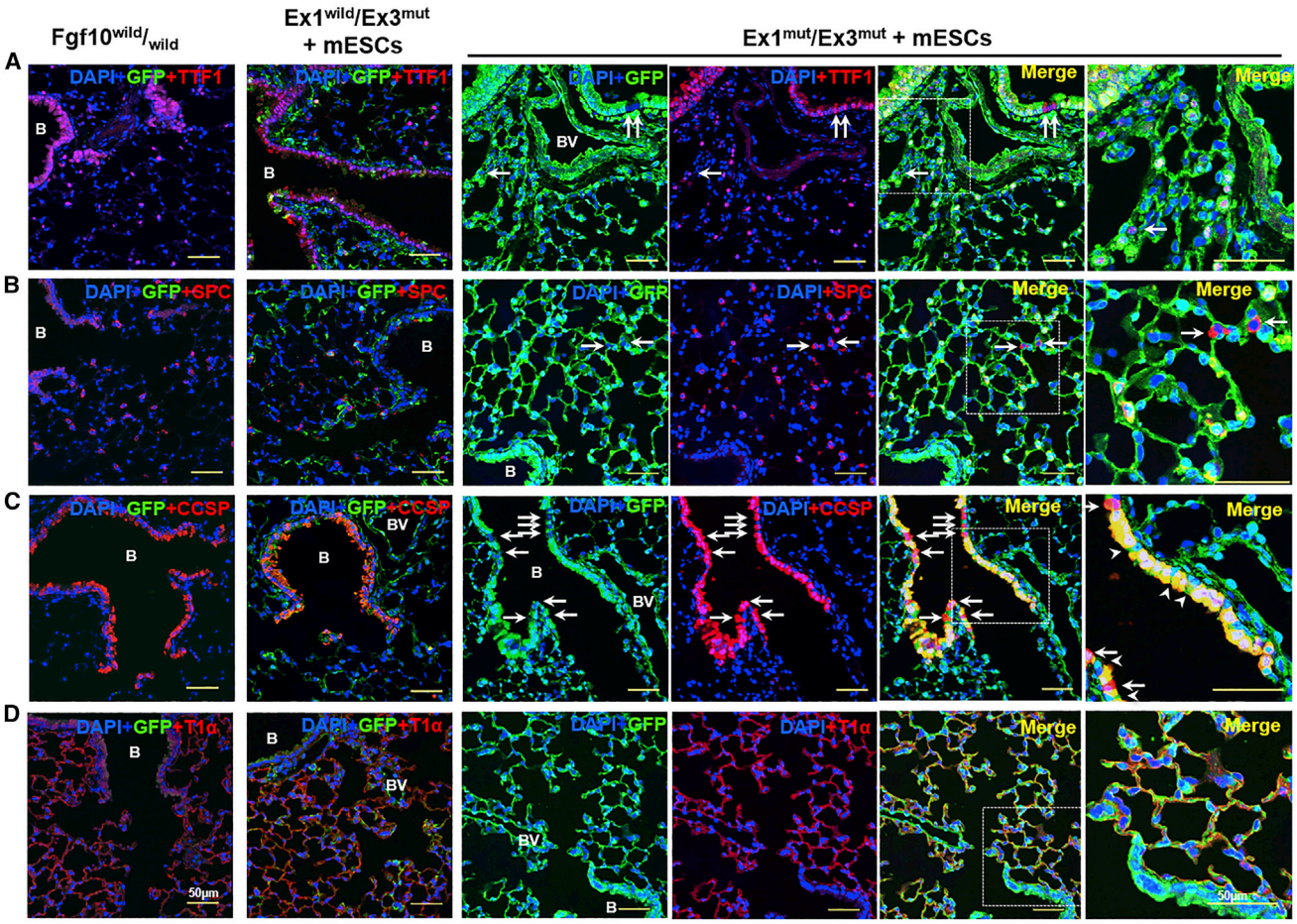

Figure 4. Immunofluorescence Staining of Parenchymal Regions of Mouse ESC-Derived Lung Tissues from Adult *Fgf10* Ex1^{mut}/Ex3^{mut} Chimeric Mice

Lung parenchyma, including the alveoli, alveolar ducts, and respiratory bronchioles, were analyzed by staining with GFP (green) together with markers for various lung lineages (red): TTF1 for type II alveolar cells and club cells (A), SPC for type II alveolar cells (B), CCSP for club cells (C), and T1α for type I alveolar cells (D). Nuclei were stained with 4′,6-diamidino-2-phenylindole (DAPI; blue). *Fgf10* $^{wild/wild}$ mice and *Fgf10* Ex1^{wild}/Ex3^{mut} chimeric mice were used as controls. The rightmost panels show magnified views of the areas indicated by dotted lines in the panels to the left. White arrows indicate GFP-negative cells of various lineages. White arrowheads indicate GFP-positive and CCSP-negative cells in terminal bronchioles. B, bronchioles; BV, blood vessel. Scale bars, 50 μm.

an ideal opportunity for exploring lung generation by blastocyst complementation.

Very recently, Mori et al. (2019) generated lungs by using mouse PSCs in Fgfr2 conditional knockout mice by blastocyst complementation. Because Fgfr2 is expressed in lung epithelial cells and is indispensable for lung morphogenesis, the proportion of GFP-positive cells was high (94.8% ± 2.1%) in lung epithelial cells but relatively low (64.3% ± 24.7%) in lung mesenchymal cells. Therefore, although lungs could be generated by blastocyst complementation in Fgfr2-knockout mice, the generated lung was composed of recipient and donor cells. Mori et al. (2019) also explored the generation of lungs in a conditional Ctnnb1-knockout mouse model and demonstrated that chimeric mice complemented with PSCs could survive to adulthood, i.e., reach full maturity, although quantitative data on the derived epithelial cells were not provided (Mori et al., 2019). In this study, we used Fgf10-knockout mice to generate lungs from mouse ESCs by blastocyst complementation. Although we generated lungs successfully, they also consisted of a mixture of recipient and donor cells.

Fgf10 is mostly secreted by the mesenchyme and exerts an effect on Fgfr2 expression in the endodermal epithelium to induce lung bud outgrowth in a paracrine fashion (Bellusci et al., 1997; Park et al., 1998; Weaver et al., 2000; Volckaert and De Langhe, 2015); this gives rise to the concern that the localized Fgf10 would act nonselectively on either GFP-positive donor cells (*Fgf10*$^{wild/wild}$) or GFP-negative host cells (*Fgf10*$^{-/-}$) resident in the endoderm. Theoretically, lung cells should be a mixture of donor and host cells. Indeed, nearly all cell types in the generated lungs of Ffg10-knockout mice were mixtures of donor and host cells. However, high proportions of donor GFP-positive cells were observed in the epithelial cells of the generated lungs, compared with the cells in other organs. This suggests a survival or differentiation advantage for lung Fgf10$^{wild/wild}$ epithelial cells

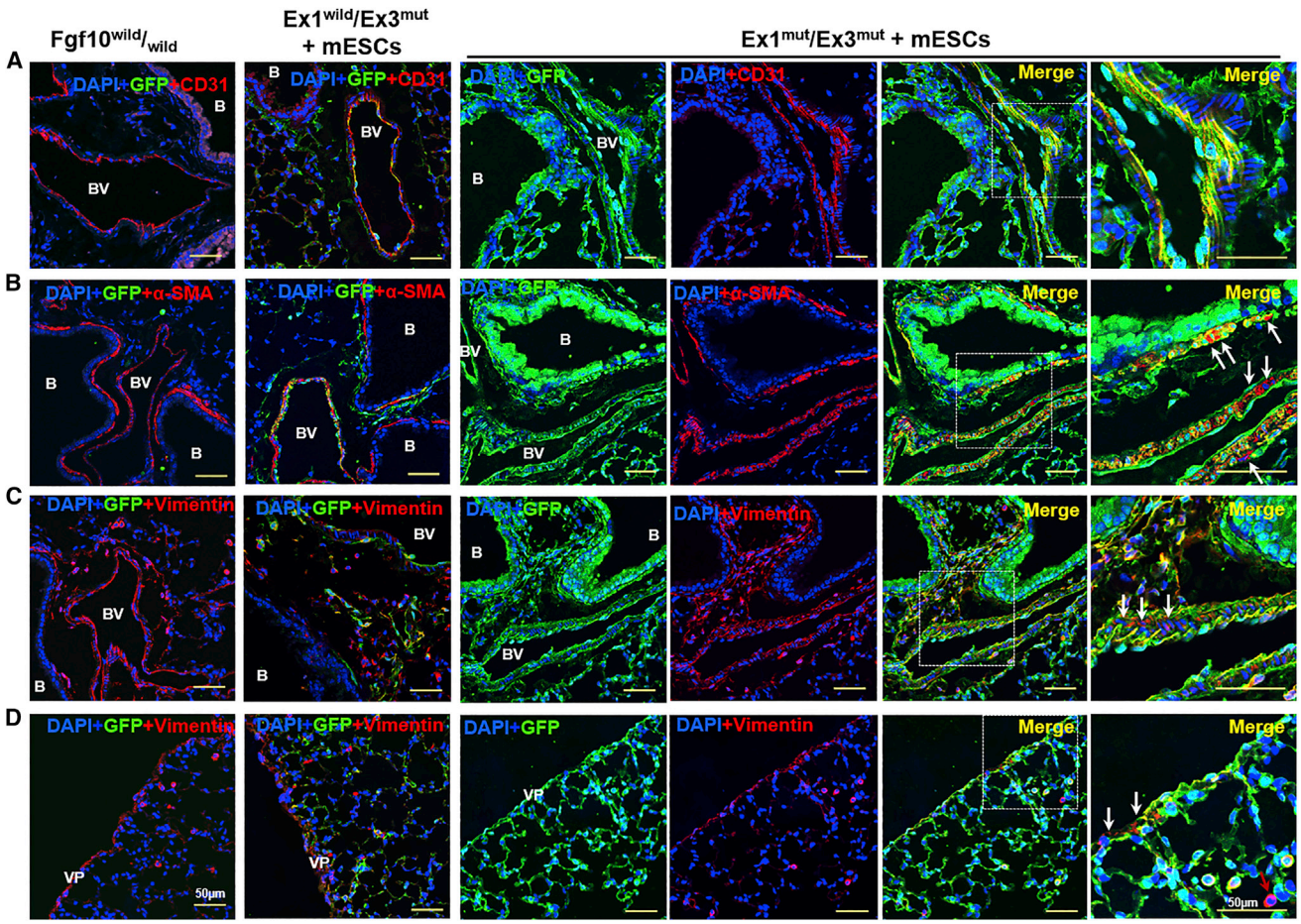

Figure 5. Immunofluorescence Staining of the Interstitial Regions of Mouse ESC-Derived Lung Tissues in Adult *Fgf10* Ex1^{mut}/Ex3^{mut} Chimeric Mice

Interstitial regions of the lung tissues were analyzed by staining with GFP (green) together with various markers (red): CD31 for vascular endothelial cells (A), α-SMA for smooth muscle cells (B), and vimentin for stromal cells (C and D). Nuclei were stained with DAPI (blue). *Fgf10* $^{wild/wild}$ and *Fgf10* Ex1^{wild}/Ex3^{mut} chimeric mice were used as controls. The rightmost panels show magnified views of the areas indicated by dotted lines in the panels to the left. White arrows indicate GFP-negative cells of various lineages. Red arrow indicates GFP-negative macrophages. B, bronchiole; BV, blood vessel; VP, visceral pleura. Scale bars, 50 μm.

compared with Fgf10 $^{mut/mut}$ cells. In contrast to the prevailing theory on the spatially localized expression of Fgf10 during lung development, ubiquitous expression of Fgf10, from the beginning of mouse lung morphogenesis (from E9.5 onward) in both the mesenchyme and epithelium on an *Fgf10*$^{-/-}$ background, has shown benefits for lung development characterized by normal lobulation and an epithelial branching pattern (Volckaert et al., 2013). Therefore, it is possible that the GFP-positive donor epithelium (*Fgf10*$^{wild/wild}$) achieves ectopic expression of Fgf10, followed by a relative preponderance in the context of lung development compared with the *Fgf10*$^{-/-}$ host epithelium. Interestingly, the interstitial cells of the lung organ generated in *Fgf10* Ex1^{mut}/Ex3^{mut} mice also predominantly originated from ESCs. These findings are supported by the accumulated knowledge about the essential role of Fgf10 in the formation of multiple mesenchymal lineages during lung development and disease. Lineage tracing of Fgf10-positive cells showed that these cells represented a pool of mesenchymal progenitors in the embryonic and postnatal lung, including progenitors of parabronchial and vascular smooth muscle cells, LIFs, and resident mesenchymal stromal cells (El Agha and Bellusci, 2014; Chao et al., 2015, 2019; El Agha et al., 2014). Autocrine Fgf10 signaling is thought to be important for controlling the differentiation of LIF progenitors and preadipocytes (Wu et al., 2018; Al Alam et al., 2015). In the hypomorphic lungs of Fgf10$^{LacZ/-}$ mice, a decline in the Fgf10 level resulted in a reduced vascular endothelial growth factor-α (VEGF-α) level and vascular defects, indicating that Fgf10 plays a pivotal role in the formation of pulmonary vasculature (Chao et al., 2019; Ramasamy et al., 2007). Embryos mutant in both Fgf10 and its major receptor Fgfr2-IIIb lack pulmonary arteries and veins (Marguerie et al., 2006). The major contribution of ESCs to the interstitial regions and parenchyma of the generated lung demonstrated in this study could inform strategies for generating PSC-derived lungs by blastocyst complementation, for modeling lung disease in large animals; there may also be applications to lung transplantation in the future.

Another concern regarding blastocyst complementation is whether the targeted genomic deficiencies in embryos are sufficiently compensated by PSCs to enable survival until adulthood and organ maturation. PSCs contributed to generating kidneys but failed to rescue the milk-suckling defect in *Sall1*$^{mut/mut}$ mice and rats, which causes death before adulthood (Usui et al., 2012; Goto et al., 2019), possibly due to the insufficient multipotency of PSCs or low proportional chimerism. In a previous report of lung generation by blastocyst complementation, *Fgfr2* or *Ctnnb1* was conditionally deleted in the foregut endoderm immediately before the onset of lung organogenesis to avoid lethality after systemic deletion, which probably occurs due to impaired trophoblast formation or multiple defects (Mori et al., 2019). Although the Fgf10-knockout mice exhibited agenesis or dysgenesis of various organs, including the lung, limb, thyroid, salivary gland, kidney, eye, thymus, and inner ear (Sekine et al., 1999; Ohuchi et al., 2000), the *Fgf10* Ex1^{mut}/Ex3^{mut} chimeric mice survived to adulthood without abnormalities. These data indicate that the Fgf10 defect could be rescued by mouse ESCs and that the generated lung was functional, although the efficacy of blastocyst complementation was low.

Given the low efficiency of generating lung organs by intraspecies blastocyst complementation (Table 1), whether PSC-derived lung organs could be generated in Fgf10-knockout rodents or livestock by interspecies blastocyst complementation remains to be investigated in a subsequent study. Efficient chimerism is considered to be the most important factor when interspecies chimeras are produced for organ generation (Okumura et al., 2019). Mouse PSCs contribute to kidney generation in rats (Goto et al., 2019), whereas rat PSCs failed to generate kidneys in anephric *Sall1* mutant mice due to their poor contribution to the metanephric mesenchyme (Usui et al., 2012). Furthermore, although human PSCs contribute to pig embryos by blastocyst injection, the level of chimerism was low and insufficient for organ generation (Wu et al., 2017). Eight-cell embryo injection increased the contribution rate of rat ESCs to chimeric mice but decreased the chimera generation rate, compared with blastocyst injection (Okumura et al., 2019). The pluripotent state affects the contribution of PSCs to xenogeneic embryos; thus, matching the developmental timing may be critical for successful chimera formation (Wu et al., 2017; Huang et al., 2018). Naive human PSCs engrafted robustly to preimplantation blastocysts but less robustly to postimplantation pig embryos, whereas human PSCs intermediate between the naive and primed states exhibited a higher degree of chimerism in postimplantation pig embryos (Wu et al., 2017). Apoptosis is a barrier to interspecies chimerism using human PSCs; also, forced expression of BMI1 (a polycomb factor) in human primed PSCs suppressed apoptosis and, thus, enabled human PSCs to integrate into preimplantation embryos of mouse, rabbit, and pig (Huang et al., 2018). The ethical issues regarding interspecies chimerism with human PSCs need to be discussed.

In summary, we generated lungs predominantly derived from mouse ESCs in apneumic *Fgf10*-knockout mice by blastocyst complementation. *Fgf10* Ex1^{mut}/Ex3^{mut} blastocysts may provide an organ developmental niche for lung generation, where *Fgf10*-deficient mice could survive until adulthood with PSC injection. The generation of PSC-derived lungs by blastocyst complementation is a promising approach for lung generation.

STAR★METHODS

Detailed methods are provided in the online version of this paper and include the following:

- KEY RESOURCES TABLE
- RESOURCE AVAILABILITY
  - Lead Contact
  - Materials Availability
  - Data and Code Availability
- EXPERIMENTAL MODEL AND SUBJECT DETAILS
  - Animals and ESCs
- METHOD DETAILS
  - Generation of Fgf10-knockout mice using the CRISPR/Cas9 system
  - Generation of chimeras with mouse ESCs
  - Genotyping of chimeras
  - Histological analysis
  - Contrast-enhanced micro-CT
- QUANTIFICATION AND STATISTICAL ANALYSIS

SUPPLEMENTAL INFORMATION

Supplemental Information can be found online at https://doi.org/10.1016/j.celrep.2020.107626.

ACKNOWLEDGMENTS

We thank Takenori Sakuma, Nae Saito, and Sumika Uchiyama for helping with the embryo manipulation, housing mice, and tail sampling. We also thank Rie Natsume for helping with the embryo microinjection and Shinichi Kenmotsu and Hayato Ohshima for helping to use the micro-CT instrument. This work was supported, in part, by the Japan Society for the Promotion of Science Grant-in-Aid for Scientific Research (KAKENHI) grant numbers 18K15921 and 18H02817G.

AUTHOR CONTRIBUTIONS

A.K. and Q.R. performed the experiments, contributed to analysis and interpretation of data, and assisted in the preparation of the manuscript. K.O. and T.S. performed the embryo manipulation and animal experiments and contributed to analysis and interpretation of mouse data. A.Y. generated the Fgf10 knockout mouse and contributed to DNA analysis. M.A. and K.S. prepared the GFP-positive mouse embryo stem cells and assisted with the embryo manipulation. X.Y. performed part of the experiments. M.T. contributed to analysis and interpretation of the data. Y.A. contributed to histological analysis and sequencing analysis. Y.S. and Q.Z. designed the research, performed part of the experiments, analyzed the data, and wrote the manuscript. All of the authors discussed the results and commented on the manuscript text.

DECLARATION OF INTERESTS

The authors declare no competing interests.

Received: February 12, 2020
Revised: April 9, 2020
Accepted: April 18, 2020
Published: May 12, 2020

REFERENCES

Al Alam, D., El Agha, E., Sakurai, R., Kheirollahi, V., Moiseenko, A., Danopoulos, S., Shrestha, A., Schmoldt, C., Quantius, J., Herold, S., et al. (2015). Evidence for the involvement of fibroblast growth factor 10 in lipofibroblast formation during embryonic lung development. Development *142*, 4139–4150.

Bellusci, S., Grindley, J., Emoto, H., Itoh, N., and Hogan, B.L. (1997). Fibroblast growth factor 10 (FGF10) and branching morphogenesis in the embryonic mouse lung. Development *124*, 4867–4878.

Chao, C.M., El Agha, E., Tiozzo, C., Minoo, P., and Bellusci, S. (2015). A breath of fresh air on the mesenchyme: impact of impaired mesenchymal development on the pathogenesis of bronchopulmonary dysplasia. Front. Med. (Lausanne) *2*, 27.

Chao, C.M., Moiseenko, A., Kosanovic, D., Rivetti, S., El Agha, E., Wilhelm, J., Kampschulte, M., Yahya, F., Ehrhardt, H., Zimmer, K.P., et al. (2019). Impact of Fgf10 deficiency on pulmonary vasculature formation in a mouse model of bronchopulmonary dysplasia. Hum. Mol. Genet. *28*, 1429–1444.

De Moerlooze, L., Spencer-Dene, B., Revest, J.M., Hajihosseini, M., Rosewell, I., and Dickson, C. (2000). An important role for the IIIb isoform of fibroblast growth factor receptor 2 (FGFR2) in mesenchymal-epithelial signalling during mouse organogenesis. Development *127*, 483–492.

El Agha, E., and Bellusci, S. (2014). Walking along the fibroblast growth factor 10 route: a key pathway to understand the control and regulation of epithelial and mesenchymal celllineage formation during lung development and repair after injury. Scientifica (Cairo) *2014*, 538379.

El Agha, E., Herold, S., Al Alam, D., Quantius, J., MacKenzie, B., Carraro, G., Moiseenko, A., Chao, C.M., Minoo, P., Seeger, W., and Bellusci, S. (2014). Fgf10-positive cells represent a progenitor cell population during lung development and postnatally. Development *141*, 296–306.

Farré, R., Otero, J., Almendros, I., and Navajas, D. (2018). Bioengineered Lungs: A Challenge and An Opportunity. Arch. Bronconeumol. *54*, 31–38.

Freedman, B.S. (2018). Hopes and Difficulties for Blastocyst Complementation. Nephron *138*, 42–47.

Ghaedi, M., Le, A.V., Hatachi, G., Beloiartsev, A., Rocco, K., Sivarapatna, A., Mendez, J.J., Baevova, P., Dyal, R.N., Leiby, K.L., et al. (2018). Bioengineered lungs generated from human iPSCs-derived epithelial cells on native extracellular matrix. J. Tissue Eng. Regen. Med. *12*, e1623–e1635.

Goss, A.M., Tian, Y., Tsukiyama, T., Cohen, E.D., Zhou, D., Lu, M.M., Yamaguchi, T.P., and Morrisey, E.E. (2009). Wnt2/2b and β-catenin signaling are necessary and sufficient to specify lung progenitors in the foregut. Dev. Cell *17*, 290–298.

Goto, T., Hara, H., Sanbo, M., Masaki, H., Sato, H., Yamaguchi, T., Hochi, S., Kobayashi, T., Nakauchi, H., and Hirabayashi, M. (2019). Generation of pluripotent stem cell-derived mouse kidneys in Sall1-targeted anephric rats. Nat. Commun. *10*, 451.

Harris-Johnson, K.S., Domyan, E.T., Vezina, C.M., and Sun, X. (2009). beta-Catenin promotes respiratory progenitor identity in mouse foregut. Proc. Natl. Acad. Sci. USA *106*, 16287–16292.

Huang, K., Zhu, Y., Ma, Y., Zhao, B., Fan, N., Li, Y., Song, H., Chu, S., Ouyang, Z., Zhang, Q., et al. (2018). BMI1 enables interspecies chimerism with human pluripotent stem cells. Nat. Commun. *9*, 4649.

Kobayashi, T., Yamaguchi, T., Hamanaka, S., Kato-Itoh, M., Yamazaki, Y., Ibata, M., Sato, H., Lee, Y.S., Usui, J., Knisely, A.S., et al. (2010). Generation of rat pancreas in mouse by interspecific blastocyst injection of pluripotent stem cells. Cell *142*, 787–799.

Lan, T., Wang, L., Xu, L., Jin, N., Yan, G., Xia, J., Wang, H., Zhuang, G., Gao, C., Meng, L., et al. (2016). Induced Pluripotent Stem Cells Can Effectively Differentiate into Multiple Functional Lymphocyte Lineages In Vivo with Negligible Bias. Stem Cells Dev. *25*, 462–471.

Marguerie, A., Bajolle, F., Zaffran, S., Brown, N.A., Dickson, C., Buckingham, M.E., and Kelly, R.G. (2006). Congenital heart defects in Fgfr2-IIIb and Fgf10 mutant mice. Cardiovasc. Res. *71*, 50–60.

Meyer, K.C. (2018). Recent advances in lung transplantation. F1000Res *7*, F1000 Faculty Rev-1684.

Mori, M., Furuhashi, K., Danielsson, J.A., Hirata, Y., Kakiuchi, M., Lin, C.-S., Ohta, M., Riccio, P., Takahashi, Y., Xu, X., et al. (2019). Generation of functional lungs via conditional blastocyst complementation using pluripotent stem cells. Nat. Med. *25*, 1691–1698.

Nichols, J.E., La Francesca, S., Niles, J.A., Vega, S.P., Argueta, L.B., Frank, L., Christiani, D.C., Pyles, R.B., Himes, B.E., Zhang, R., et al. (2018). Production and transplantation of bioengineered lung into a large-animal model. Sci Transl Med. *10*, eaao3926.

Ohuchi, H., Hori, Y., Yamasaki, M., Harada, H., Sekine, K., Kato, S., and Itoh, N. (2000). FGF10 acts as a major ligand for FGF receptor 2 IIIb in mouse multi-organ development. Biochem. Biophys. Res. Commun. *277*, 643–649.

Okumura, H., Nakanishi, A., Toyama, S., Yamanoue, M., Yamada, K., Ukai, A., Hashita, T., Iwao, T., Miyamoto, T., Tagawa, Y.I., et al. (2019). Contribution of rat embryonic stem cells to xenogeneic chimeras in blastocyst or 8-cell embryo injection and aggregation. Xenotransplantation *26*, e12468.

Ott, H.C., Clippinger, B., Conrad, C., Schuetz, C., Pomerantseva, I., Ikonomou, L., Kotton, D., and Vacanti, J.P. (2010). Regeneration and orthotopic transplantation of a bioartificial lung. Nat. Med. *16*, 927–933.

Park, W.Y., Miranda, B., Lebeche, D., Hashimoto, G., and Cardoso, W.V. (1998). FGF-10 is a chemotactic factor for distal epithelial buds during lung development. Dev. Biol. *201*, 125–134.

Petersen, T.H., Calle, E.A., Zhao, L., Lee, E.J., Gui, L., Raredon, M.B., Gavrilov, K., Yi, T., Zhuang, Z.W., Breuer, C., et al. (2010). Tissue-engineered lungs for in vivo implantation. Science *329*, 538–541.

Ramasamy, S.K., Mailleux, A.A., Gupte, V.V., Mata, F., Sala, F.G., Veltmaat, J.M., Del Moral, P.M., De Langhe, S., Parsa, S., Kelly, L.K., et al. (2007). Fgf10 dosage is critical for the amplification of epithelial cell progenitors and for the formation of multiple mesenchymal lineages during lung development. Dev. Biol. *307*, 237–247.

Rashid, T., Kobayashi, T., and Nakauchi, H. (2014). Revisiting the flight of Icarus: making human organs from PSCs with large animal chimeras. Cell Stem Cell *15*, 406–409.

Sekine, K., Ohuchi, H., Fujiwara, M., Yamasaki, M., Yoshizawa, T., Sato, T., Yagishita, N., Matsui, D., Koga, Y., Itoh, N., and Kato, S. (1999). Fgf10 is essential for limb and lung formation. Nat. Genet. *21*, 138–141.

Song, J.J., Kim, S.S., Liu, Z., Madsen, J.C., Mathisen, D.J., Vacanti, J.P., and Ott, H.C. (2011). Enhanced in vivo function of bioartificial lungs in rats. Ann. Thorac. Surg. *92*, 998–1005, discussion 1005–1006.

Usui, J., Kobayashi, T., Yamaguchi, T., Knisely, A.S., Nishinakamura, R., and Nakauchi, H. (2012). Generation of kidney from pluripotent stem cells via blastocyst complementation. Am. J. Pathol. *180*, 2417–2426.

Volckaert, T., and De Langhe, S.P. (2015). Wnt and FGF mediated epithelial-mesenchymal crosstalk during lung development. Dev. Dyn. *244*, 342–366.

Volckaert, T., Campbell, A., Dill, E., Li, C., Minoo, P., and De Langhe, S. (2013). Localized Fgf10 expression is not required for lung branching morphogenesis but prevents differentiation of epithelial progenitors. Development *140*, 3731–3742.

Weaver, M., Dunn, N.R., and Hogan, B.L. (2000). Bmp4 and Fgf10 play opposing roles during lung bud morphogenesis. Development *127*, 2695–2704.

Wu, J., Platero-Luengo, A., Sakurai, M., Sugawara, A., Gil, M.A., Yamauchi, T., Suzuki, K., Bogliotti, Y.S., Cuello, C., Morales Valencia, M., et al. (2017). Interspecies chimerism with mammalian pluripotent stem cells. Cell *168*, 473–486.e15.

Wu, J., Chu, X., Chen, C., and Bellusci, S. (2018). Role of fibroblast growth factor 10 in mesenchymal cell differentiation during lung development and disease. Front. Genet. *9*, 545.

Yamaguchi, T., Sato, H., Kato-Itoh, M., Goto, T., Hara, H., Sanbo, M., Mizuno, N., Kobayashi, T., Yanagida, A., Umino, A., et al. (2017). Interspecies

organogenesis generates autologous functional islets. Nature *542*, 191–196.

Yasue, A., Mitsui, S.N., Watanabe, T., Sakuma, T., Oyadomari, S., Yamamoto, T., Noji, S., Mito, T., and Tanaka, E. (2014). Highly efficient targeted mutagenesis in one-cell mouse embryos mediated by the TALEN and CRISPR/Cas systems. Sci. Rep. *4*, 5705.

Yuan, T., Volckaert, T., Chanda, D., Thannickal, V.J., and De Langhe, S.P. (2018). Fgf10 signaling in lung development, homeostasis, disease, and repair after injury. Front. Genet. *9*, 418.

Zhou, Q., Ye, X., Sun, R., Matsumoto, Y., Moriyama, M., Asano, Y., Ajioka, Y., and Saijo, Y. (2014). Differentiation of mouse induced pluripotent stem cells into alveolar epithelial cells in vitro for use in vivo. Stem Cells Transl. Med. *3*, 675–685.

STAR★METHODS

KEY RESOURCES TABLE

REAGENT or RESOURCE	SOURCE	IDENTIFIER
Antibodies		
Rabbit anti-GFP polyclonal antibody	Abcam	Cat#ab290; RRID:AB_303395
Goat anti-GFP polyclonal antibody	GeneTex	Cat#GTX26673; RRID:AB_371426
Rabbit anti-TTF1 monoclonal antibody; Clone EP1584Y	Abcam	Cat#ab76013; RRID:AB_1310784
Rabbit anti-SPC monoclonal antibody	Abcam	Cat#ab211326
Rabbit anti-CD31 polyclonal antibody	Novus Biologicals	Cat#NB100-2284; RRID:AB_10002513
Goat anti-CCSP polyclonal antibody	Santa Cruz Biotechnology	Cat#sc-9772; RRID:AB_2238819
Goat anti-T1α polyclonal antibody	Santa Cruz Biotechnology	Cat#sc-23564; RRID:AB_2161941
Rabbit anti-αSMA polyclonal antibody	Abcam	Cat#ab5694; RRID:AB_2223021
Rabbit anti-βIII-tubulin antibody	Abcam	Cat#ab18207; RRID:AB_444319
Donkey anti-rabbit IgG-Alexa Fluor 488	Invitrogen	Cat#A21206; RRID:AB_2535792
Donkey anti-goat IgG-Alexa Fluor 488	Invitrogen	Cat#A11055; RRID:AB_2534102
Donkey anti-rabbit IgG-Alexa Fluor 594	Invitrogen	Cat#A21207; RRID:AB_141637
Donkey anti-goat IgG-Alexa Fluor 594	Invitrogen	Cat#A11058; RRID:AB_142540
Chemicals, Peptides, and Recombinant Proteins		
Mitomycin C	Sigma-Aldrich	Cat#M0503
Knockout-DMEM	GIBCO	Cat#10829-018
Fetal bovine serum	Cambrex	Cat#14-502FM; Lot.SF50602
Knockout Serum Replacement	GIBCO	Cat#10828-028; Lot.1123784
Nonessential amino acids	GIBCO	Cat#11140-050
L-glutamine	GIBCO	Cat#25030-081
2-mercaptoethanol	Sigma-Aldrich	Cat#M7522
mLIF	Merck	Cat#ESG1107 ESGRO
Critical Commercial Assays		
DNeasy Blood & Tissue kits	QIAGEN	Cat#69504
KOD-Plus-Neo kits	Toyobo	Cat#KOD-401
Wizard SV Gel and PCR Clean-up system	Promega	Cat#A9282
Surveyor Mutation Detection kit	Transgenomic	Cat#706020
BigDye Terminator Cycle Sequencing kit	ThermoFisher	Cat#4337455
Experimental Models: Cell Lines		
GFP-expressing mouse RENKA C57BL/6NCrlCrlj ESCs	Niigata University	CFS-EGFP27
Experimental Models: Organisms/Strains		
Mouse: BDF1	CLEA	N/A
Oligonucleotides		
Primer: Fgf10 Ex1 Forward: 5′-CAGCAGGTCTTACCCTTCCA-3′	Yasue et al., 2014	N/A
Primer: Fgf10 Ex1 Reverse: 5′-TACA GGGGTTGGGGACATAA-3′	Yasue et al., 2014	N/A
Primer: Fgf10 Ex3 Forward: 5′-TGACTCTTCTGTTGTTAGCGT TG-3′	Yasue et al., 2014	N/A
Primer: Fgf10 Ex3 Reverse: 5′-ACATCCAAAGCCTTCCTTCC-3′	Yasue et al., 2014	N/A
Recombinant DNA		
Cas9 mRNA and sgRNA	Yasue et al., 2014	N/A
Software and Algorithms		
TRI/3D-Bon software	Ratoc System Engineering	N/A

RESOURCE AVAILABILITY

Lead Contact

Further information and requests for resources and reagents should be directed to and will be fulfilled by the Lead Contact, Qiliang Zhou (zhouql@med.niigata-u.ac.jp).

Materials Availability

This study did not generate new unique reagents.

Data and Code Availability

This study did not generate any unique datasets or code.

EXPERIMENTAL MODEL AND SUBJECT DETAILS

Animals and ESCs

Animal care and procedures were approved by the Institutional Animal Care and Use Committee of Niigata University, Niigata, Japan (approval number, SA00233). All animals in this study were housed under specific pathogen-free conditions in a 12h light/dark cycle at 25°C, with food and water available *ad libitum*. Eight-week-old pathogen-free female mice with the BDF1 genetic background were purchased from CLEA Japan, Inc. (Tokyo, Japan). GFP-expressing mouse RENKA C57BL/6NCrlCrlj ESCs (#CFS-EGFP27; Brain Research Institute, Niigata University) were maintained on mitomycin C (Sigma-Aldrich, St. Louis, MO)-treated primary cultured mouse embryonic fibroblasts in KO-ES medium consisting of knockout-Dulbecco's modified Eagle's medium (GIBCO, Carlsbad, CA) with 8.8% fetal bovine serum (Cambrex, Charles City, IA), 8.8% Knockout Serum Replacement (GIBCO), 88 μM nonessential amino acids (GIBCO), 1.8 mM L-glutamine (GIBCO), 88 μM 2-mercaptoethanol (Sigma-Aldrich), and 884 U/mL mLIF (Merck, Burlington, MA). All cell cultures were grown at 37°C and 5% CO2.

METHOD DETAILS

Generation of Fgf10-knockout mice using the CRISPR/Cas9 system

Fgf10-knockout mice were generated using the CRISPR/Cas9 system as described previously (Yasue et al., 2014). Fertilized mouse eggs were harvested from superovulated BDF1 female mice crossed with males of the same strain at 0.5 days postcoitum (dpc). Cas9 mRNAs and single-guide RNAs with the target sequence of *Fgf10* Ex1 or Ex3 (targets 1 and 2 in Figure 1, respectively) were produced by *in vitro* transcription using *Pme*I-digested Cas9 and *Dra*I-digested gRNA expression vectors and subsequently microinjected into the cytoplasm of fertilized mouse eggs. Injected eggs were cultured overnight in M16 medium at 37°C under 5% CO_2 in air, and two-cell embryos were transferred into the oviducts of pseudopregnant females. Genomic DNA was extracted from the tail tips of founder mice and used for the detection of the CRISPR-induced mutation at the *Fgf10* locus.

Generation of chimeras with mouse ESCs

Mouse ESCs expressing GFP (RENKA C57BL/6NCrlCrlj; #CFS-EGFP27) were used for blastocyst injection. Embryos were prepared via *in vitro* fertilization with *Fgf10* Ex3 -/+ ova and *Fgf10* Ex1 -/+ sperm. Five to eight ESCs were microinjected into the perivitelline space of eight-cell/morula-stage embryos (2.5 days post fertilization). After injection, the embryos were cultured in KSOM-AA medium (ARK Resource Co., Ltd. Kumamoto, Japan) for 20 h until they developed to the blastocyst stage. The embryos were thereafter transferred into the uteri of pseudopregnant recipient ICR female mice (2.5 dpc).

Genotyping of chimeras

Genotyping using the Surveyor® System and DNA sequencing were carried out as described previously (Yasue et al., 2014). Briefly, genomic DNA was extracted from the tail or other tissues using DNeasy Blood & Tissue kits (QIAGEN, Valencia, CA) and PCR was carried out using KOD-Plus-Neo kits (Toyobo, Osaka, Japan) according to the manufacturers' protocols. The PCR primers used to amplify *Fgf10* Ex1 and Ex3, respectively, were as follows: Ex1F 5′-CAGCAGGTCTTACCCTTCCA-3′ and Ex1R 5′-TACA GGGGTTGGGGACATAA-3′ (521 bp); and Ex3F 5′-TGACTCTTCTGTTGTTAGCGT TG-3′ and Ex3R 5′-ACATCCAAAGCCT TCCTTCC-3′ (501 bp). PCR products were purified using the Wizard SV Gel and PCR Clean-up system (Promega, Madison, WI), digested at mismatched sites by Surveyor Nuclease S using a Surveyor Mutation Detection kit (Transgenomic, Omaha, NE), and resolved using electrophoresis in agarose gels. Purified PCR products were subjected to DNA sequencing using a BigDye Terminator Cycle Sequencing kit and the ABI 3500 Genetic Analyzer (Applied Biosystems, Foster City, CA).

Histological analysis

Mouse tissues were fixed in 4% paraformaldehyde or 10% neutral buffered formalin and embedded in Optimal Cutting Temperature compound or paraffin. Paraffin-embedded sections were deparaffinized with xylene and hydrated in a graded ethanol series. Next, H&E staining or immunofluorescence staining was performed as described previously (Zhou et al., 2014). The primary antibodies

were: anti-GFP polyclonal antibody (rabbit IgG, 1:200; Abcam, Cambridge, UK; #ab290), anti-GFP polyclonal antibody (goat IgG, 1:200; GeneTex, Irvine, CA; #GTX26673), anti-TTF1 monoclonal antibody (rabbit IgG, 1:200; Abcam; #ab76013), anti-SPC monoclonal antibody (rabbit IgG, 1:200; Abcam; #ab211326), anti-CD31 polyclonal antibody (rabbit IgG, 1:100; Novus Biologicals, Centennial, CO; #NB100-2284), anti-CCSP polyclonal antibody (goat IgG, 1:200; Santa Cruz Biotechnology, Dallas, TX; #sc-9772), anti-T1α polyclonal antibody (goat IgG, 1:200; Santa Cruz Biotechnology; #sc-23564), anti-αSMA polyclonal antibody (rabbit IgG, 1:100; Abcam; #ab5694), and anti-βIII-tubulin antibody (rabbit IgG, 1:200; Abcam; #ab18207). Donkey anti-rabbit IgG-Alexa Fluor 488 (1:200; Invitrogen, Carlsbad, CA; #A21206), donkey anti-goat IgG-Alexa Fluor 488 (1:200; Invitrogen; #A11055), donkey anti-rabbit IgG-Alexa Fluor 594 (1:200; Invitrogen; #A21207), and donkey anti-goat IgG-Alexa Fluor 594 (1:200; Invitrogen; #A11058) were used as secondary antibodies. Nuclei were counterstained with 4′,6-diamidino-2-phenylindole (DAPI) and fluorescence images were acquired using a C1si confocal microscope (Nikon, Tokyo, Japan).

SPC- and CCSP-positive cells were enumerated in at least 20 images (200 × magnification for SPC-positive cells and 400 × for CCSP-positive cells) randomly selected from the five lung lobes.

Contrast-enhanced micro-CT

To evaluate the lung deficiencies in *Fgf10* Ex1^{mut}/Ex3^{mut} neonatal mice and lung formation in *Fgf10* Ex1^{mut}/Ex3^{mut} chimeric neonatal mice, contrast-enhanced micro-CT was used. Samples from neonatal mice were fixed in 4% paraformaldehyde at 4°C for 2 days. After detaching the epidermis, the samples were immersed in 25% Lugol's iodine solution (12.5 mg of iodine and 25 mg of potassium iodide per milliliter of distilled water) at room temperature for 1 week. Subsequently, the samples were scanned using a micro-CT device (Nittetsu Elex, Tokyo, Japan) and analyzed with TRI/3D-Bon software (Ratoc System Engineering Co., Ltd. Tokyo, Japan).

QUANTIFICATION AND STATISTICAL ANALYSIS

Body weights of neonatal mice in 5 groups (n = 3-15) are measured. Data are presented as the means ± standard deviation. The Tukey–Kramer test was used to assess the significance of differences. A *P*-value of < 0.05 was deemed to indicate significance.

Cell Reports, Volume *31*

Supplemental Information

Generation of Lungs by Blastocyst Complementation in Apneumic Fgf10-Deficient Mice

Akihiko Kitahara, Qingsong Ran, Kanako Oda, Akihiro Yasue, Manabu Abe, Xulu Ye, Toshikuni Sasaoka, Masanori Tsuchida, Kenji Sakimura, Yoichi Ajioka, Yasuo Saijo, and Qiliang Zhou

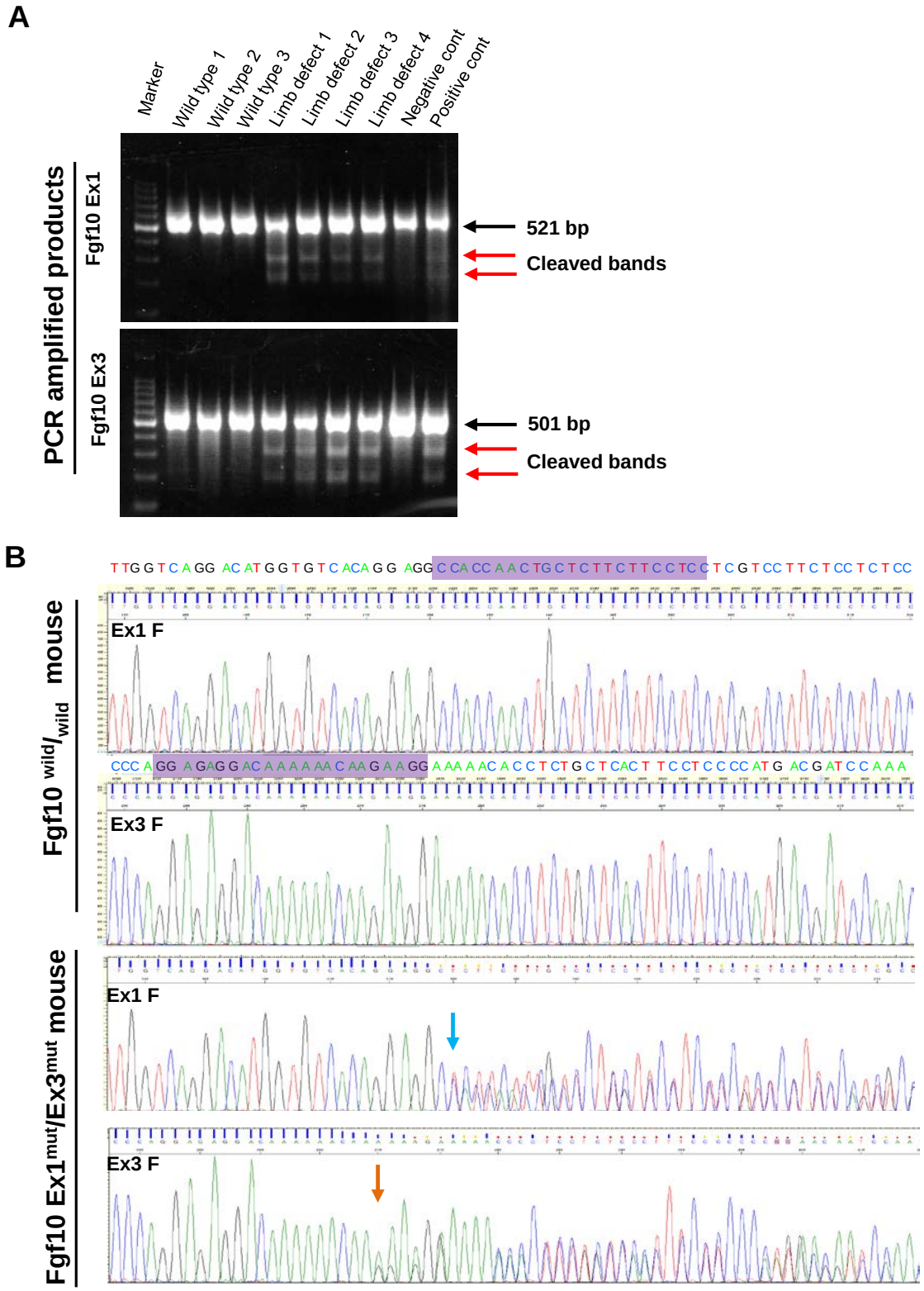

Figure S1. DNA analyses of the *Fgf10* Ex1^{mut}/Ex3^{mut} neonatal mice. Related to Figure 1.

(A) Surveyor endonuclease assay of limb-defect neonates from *Fgf10* Ex1^{mut}/Ex3^{wild} × Ex1^{wild}/Ex3^{mut} compared with *Fgf10* $^{wild}/_{wild}$ mice. The PCR products of *Fgf10* Ex1 and Ex3 consist of 521 and 501 base pairs, respectively. Cleaved bands indicate heterozygous PCR amplicons. Samples from limb-defect mice produced cleaved bands for the Ex1 and Ex3 PCR products, indicating a compound heterozygous genetic background (*Fgf10* Ex1^{mut}/Ex3^{mut}).

(B) DNA sequence analyses of the limb-defect neonates. The target sequences of the CRISPR/Cas9 system are highlighted in purple. Blue and orange arrows indicate the deletion and insertion points in the Ex1 and Ex3 forward sequences, respectively.

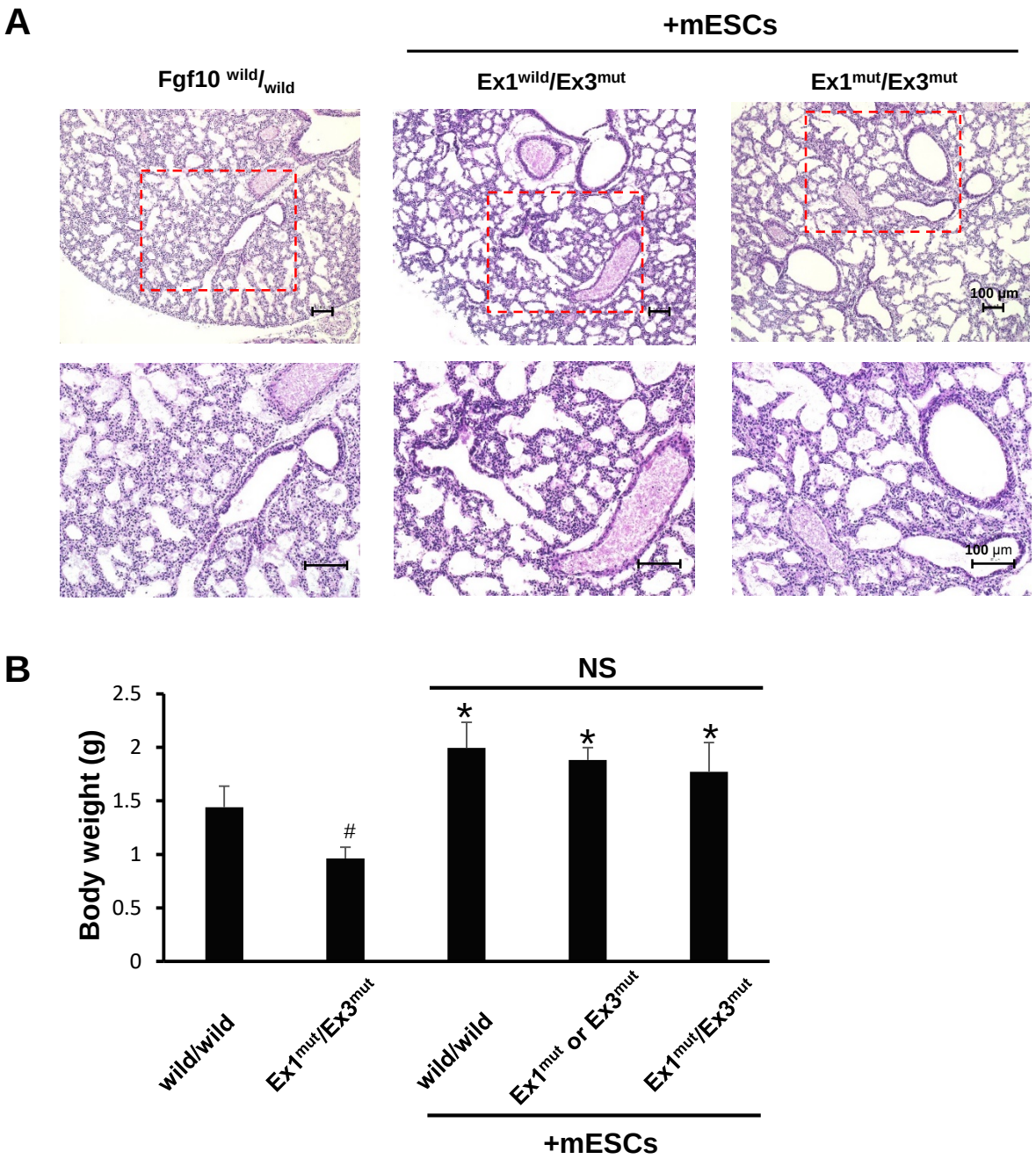

Figure S2. Characterization of the neonatal mice. Related to Figure 2.

(A) H&E staining of lung tissues from neonatal *Fgf10* $^{wild}/_{wild}$ mice, and Ex1^{wild}/Ex3^{mut} and Ex1^{mut}/Ex3^{mut} chimeric mice. Scale bars = 100 μm.

(B) Analysis of body weight in *Fgf10* $^{wild}/_{wild}$ (n=15), Ex1^{mut}/Ex3^{mut} (n=7) neonates and chimeric *Fgf10* $^{wild}/_{wild}$ (n=13), Ex1^{mut} or Ex3^{mut} (n=3), Ex1^{mut}/Ex3^{mut} (n=5) neonates. All data were obtained from 4 independent experiments. Data are represented as mean ± SD. **P* <0.05, *versus Fgf10* $^{wild}/_{wild}$ neonates; $^{\#}$*P* <0.01, *versus* other treatments; NS: statistically non-significant: *P* >0.05.

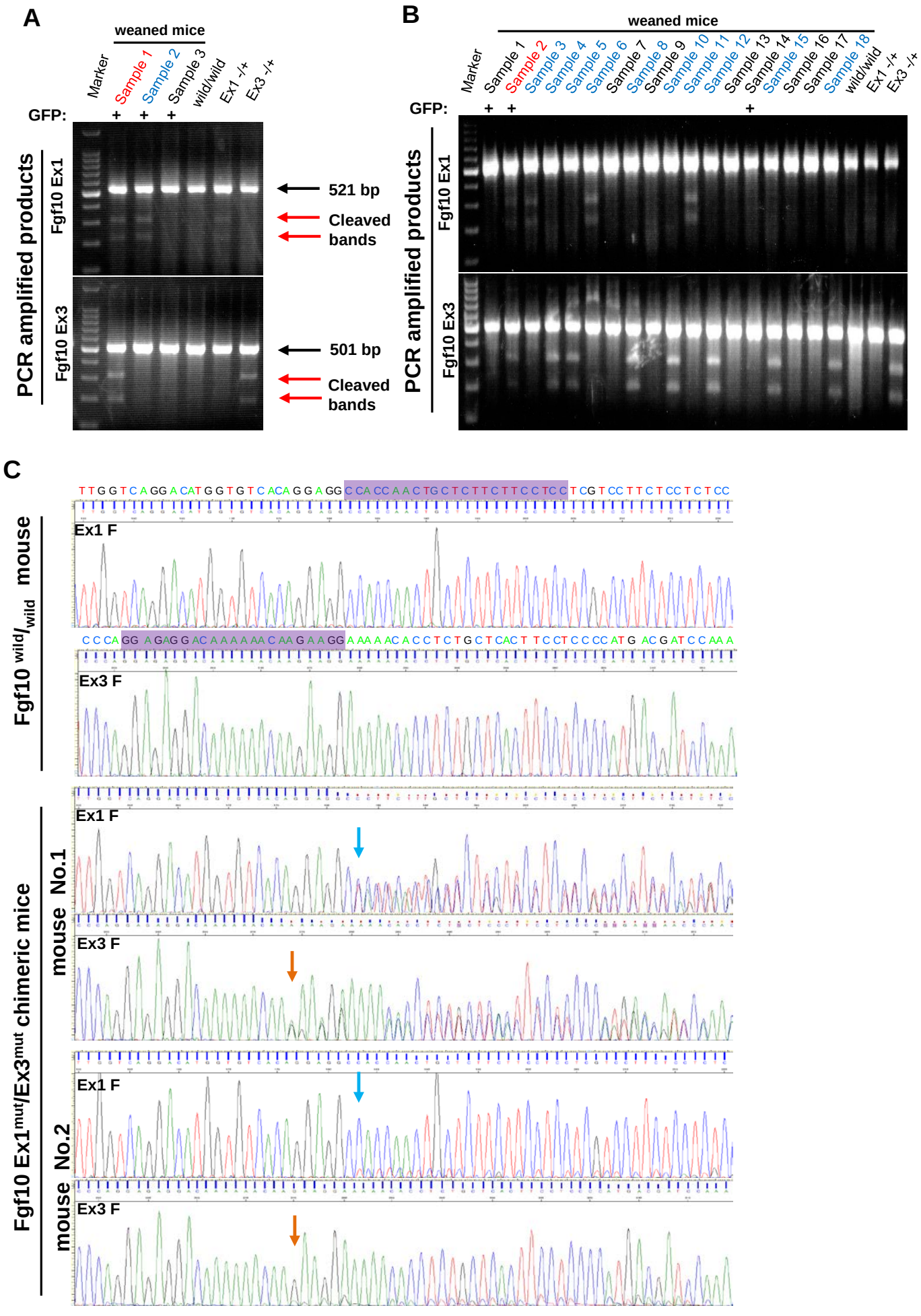
A
weaned mice
Marker
Sample 1
Sample 2
Sample 3
wild/wild
Ex1 -/+
Ex3 -/+
GFP:
+ + +
PCR amplified products
Fgf10 Ex1
Fgf10 Ex3
521 bp
Cleaved bands
501 bp
Cleaved bands
B
weaned mice
Marker
Sample 1
Sample 2
Sample 3
Sample 4
Sample 5
Sample 6
Sample 7
Sample 8
Sample 9
Sample 10
Sample 11
Sample 12
Sample 13
Sample 14
Sample 15
Sample 16
Sample 17
Sample 18
wild/wild
Ex1 -/+
Ex3 -/+
GFP:
+ + +
PCR amplified products
Fgf10 Ex1
Fgf10 Ex3
C
Fgf10 wild/wild mouse
Ex1 F
Ex3 F
Fgf10 Ex1mut/Ex3mut chimeric mice
mouse No.1
Ex1 F
Ex3 F
mouse No.2
Ex1 F
Ex3 F

Figure S3. DNA analyses of the weaned chimeric mice. Related to Figure 3.
Equal amounts of DNA templates extracted from the tail were used.
(A) and (B) Surveyor endonuclease assay. Samples were collected from the weaned mice in Experiments 1 (A), 4, and 5 (B), as described in supplementary Table 3. The PCR products of *Fgf10* Ex1 and Ex3 consist of 521 and 501 base pairs, respectively. Cleaved bands indicate heterozygous PCR amplicons. Samples from mouse No. 1 (A) and No. 2 (B) (red text) produced cleaved bands for the Ex1 and Ex3 PCR products, indicating a compound heterozygous genetic background (*Fgf10* $Ex1^{mut}/Ex3^{mut}$). Blue text indicates Ex1 or Ex3 heterozygous samples.
(C) DNA sequence analyses of the weaned compound heterozygous chimeric mice. The target sequences of the CRISPR/Cas9 system are highlighted in purple. Blue and orange arrows indicate the deletion and insertion points in the Ex1 and Ex3 forward sequences, respectively.

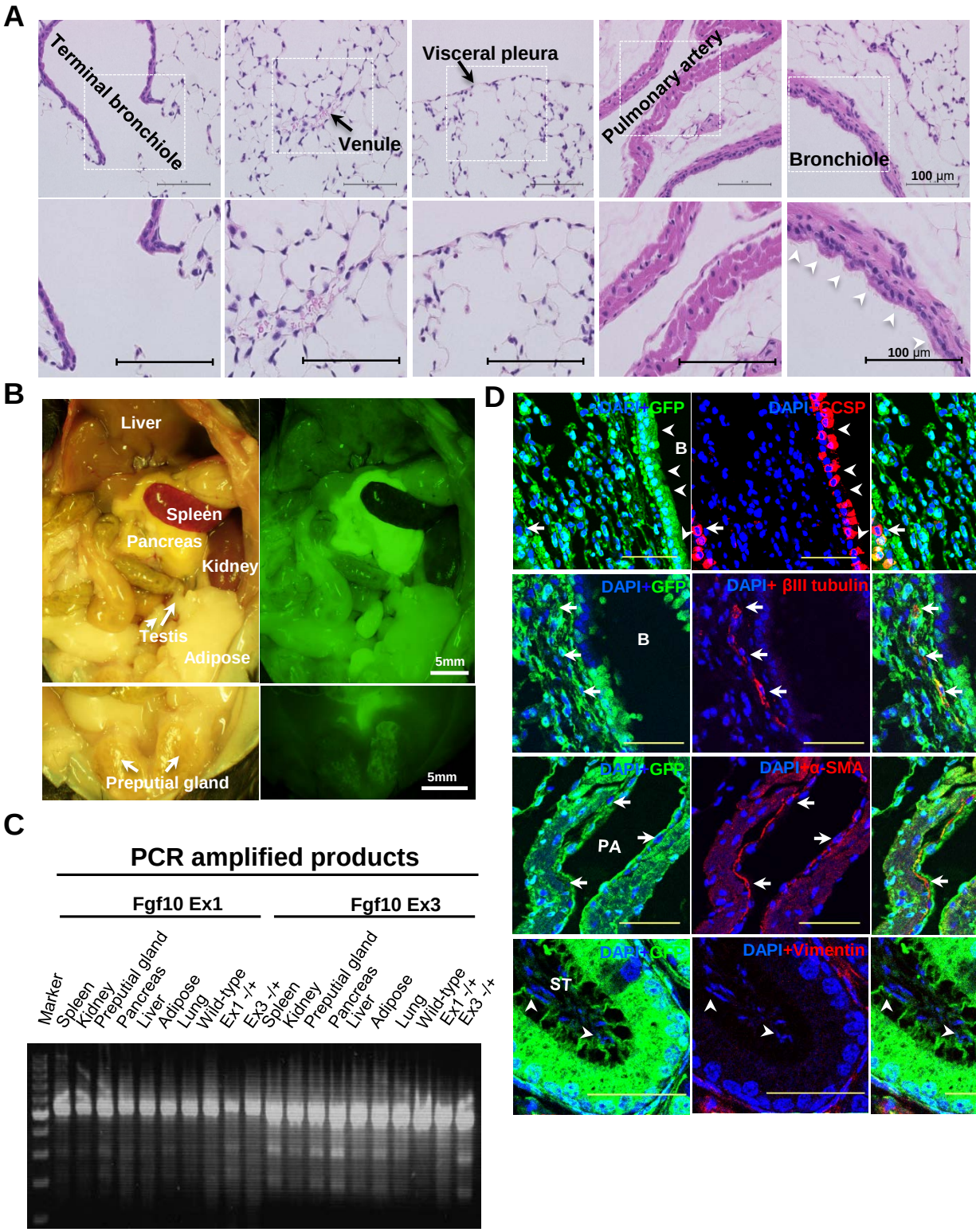

Figure S4. Characterization of weaned *Fgf10* Ex1^{mut}/Ex3^{mut} chimeric mice complemented with ESCs. Related to Figure 3-5.

(A) Histological analysis of portions of ESC-derived lung tissues stained with H&E. White arrowheads indicate ciliated cells. Scale bars = 100 μm.

(B) and (C) Contribution of mouse ESCs to various organs in *Fgf10* Ex1^{mut}/Ex3^{mut} chimeric mice. (B) Stereomicroscopic bright-field and fluorescence images. (C) Surveyor endonuclease assay of tissue samples.

(D) Immunofluorescence staining of lung tissues from adult *Fgf10* Ex1^{mut}/Ex3^{mut} chimeric mice using GFP (green) and stains for the following markers (red): CCSP for club cells, βIII-tubulin for nerve cells, and α-SMA for smooth muscle cells. Nuclei were stained with DAPI (blue). White arrows indicate GFP-negative cells of various lineages. White arrowheads indicate GFP-positive ciliary cells and sperm cells in bronchioles and seminiferous tubule, respectively. B, bronchioles; PA, pulmonary artery; ST, seminiferous tubule. Scale bars = 50 μm.

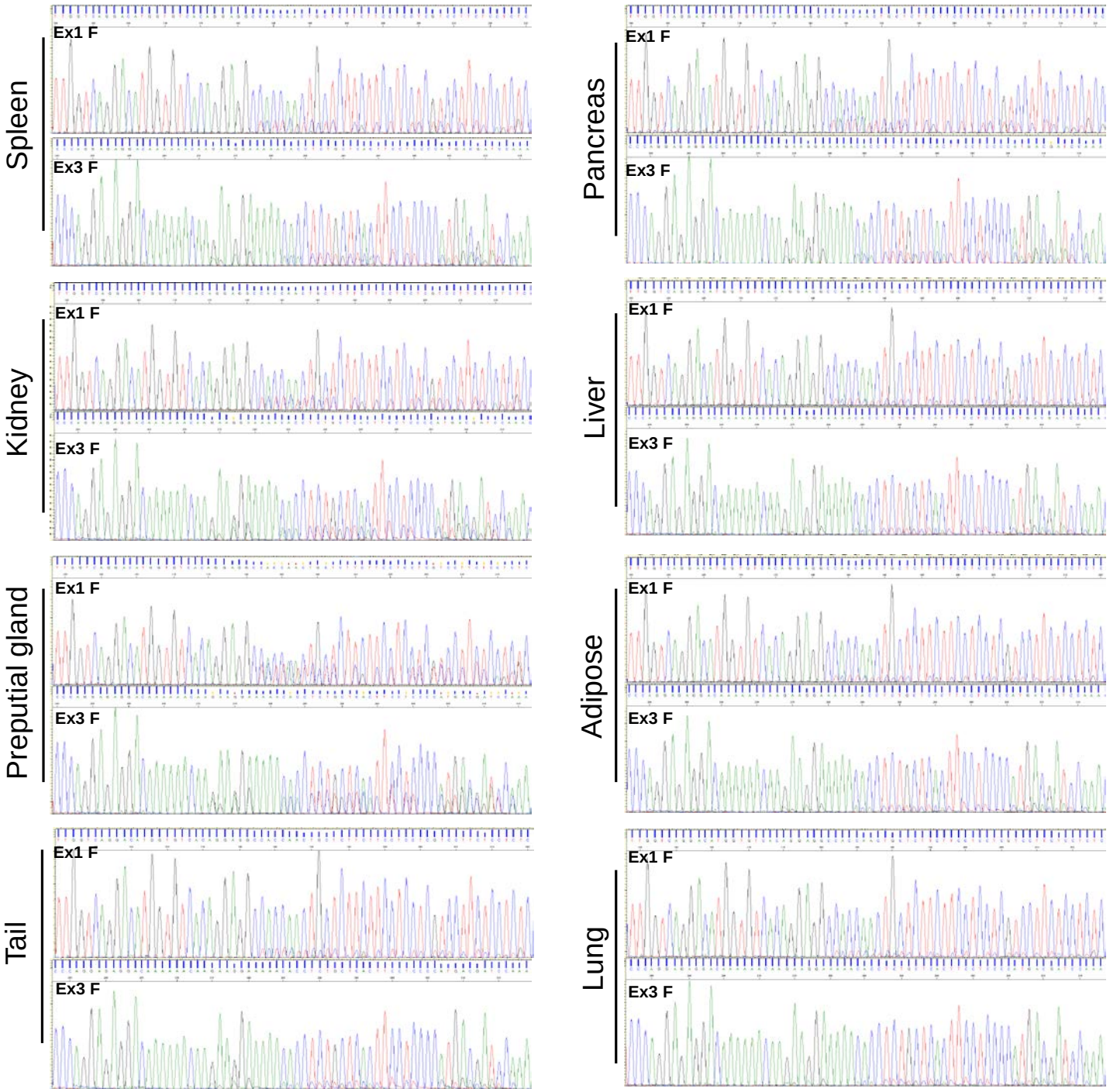

Figure S5. DNA sequence analysis of tissue samples from weaned *Fgf10* Ex1^{mut}/Ex3^{mut} chimeric mice. Related to Figure 3-5.

The DNA sequences indicated that ESCs contributed to all organs to different degrees.

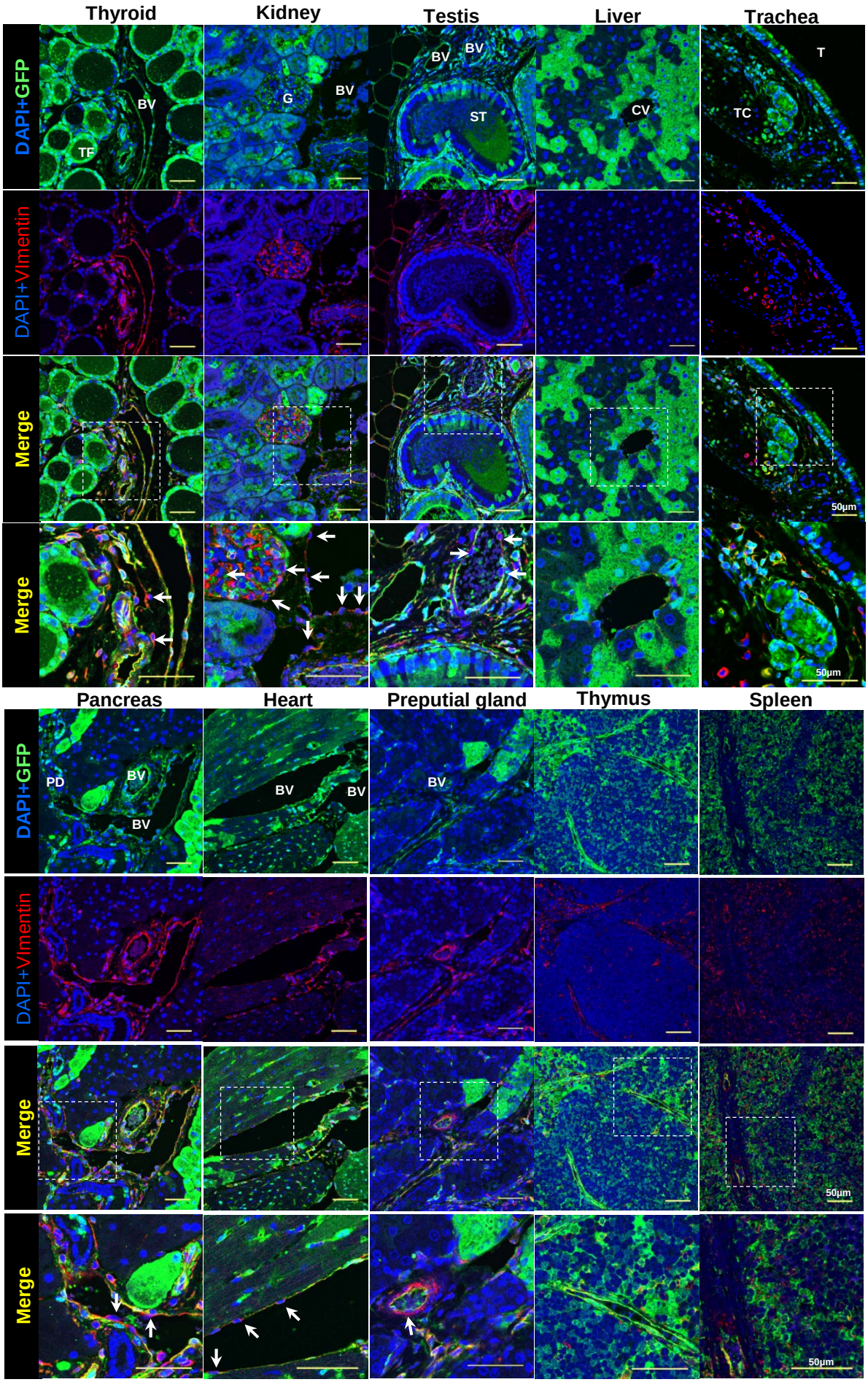
Thyroid
Kidney
Testis
Liver
Trachea
DAPI+GFP
DAPI+Vimentin
Merge
Merge
BV
TF
G
BV
BV
BV
ST
CV
T
TC
50μm
50μm
Pancreas
Heart
Preputial gland
Thymus
Spleen
DAPI+GFP
DAPI+Vimentin
Merge
Merge
PD
BV
BV
BV
BV
BV
50μm
50μm

Figure S6. Contribution of mouse ESCs to various organs in adult *Fgf10* Ex1^{mut}/Ex3^{mut} chimeric mice. Related to Figure 3-5.

Immunofluorescence staining of organs from weaned *Fgf10* Ex1^{mut}/Ex3^{mut} chimeric mice. The bottom panels show magnified views of the areas demarcated by dotted lines in the panels above. White arrows indicate GFP-negative cells of various lineages. TF, thyroid follicle; BV, blood vessel; G, glomerulus; ST, seminiferous tubule; CV, central vein of liver; T, trachea; TC, tracheal cartilage; PD, pancreatic duct. Scale bars = 50 μm.

Table S1. Controls for generation of Fgf10 Ex1^{mut}/Ex3^{mut} mice without blastocyst complementation. Related to Figure 1 and Table 1.

		Exp1	Exp2	Exp3	Total
Blastocyst transferred		26	25	13	64
Fetuses		7	6	6	19
Phenotype	Normal	7	2	6	15
	Limb defect	0	4	0	4
Genotype	Fgf10 $^{wild}/_{wild}$	2	0	2	4
	Ex1^{mut}/Ex3^{wild}	3	1	1	5
	Ex1^{wild}/Ex3^{mut}	2	1	3	6
	Ex1^{mut}/Ex3^{mut}	0	4	0	4

Table S2. Results of blastocyst complementation for lung generation at the neonatal stage. Related to Table 1.

		Exp1	Exp2	Exp3	Exp4	Total
Blastocysts injected		26	24	25	47	122
Blastocysts transferred		26	24	25	46	121
Fetuses		12	7	13	11	43 (36%)
Phenotype	Normal	10	7	8	11	36
	Limb defect	2	0	5	0	7
Genotype	Fgf10 $^{wild}/_{wild}$	3	3	5	6	17
	Ex1^{mut}/Ex3^{wild}	2	2	1	2	7
	Ex1^{wild}/Ex3^{mut}	4	1	1	1	7
	Ex1^{mut}/Ex3^{mut}	3	1	6	2	12
Chimeric fetuses		3	4	4	9	20 (47%)
Phenotype	Normal	3	4	4	9	20
	Limb defect	0	0	0	0	0
Genotype	Fgf10 $^{wild}/_{wild}$	1	2	3	6	12
	Ex1^{mut}/Ex3^{wild}	0	0	0	1	1
	Ex1^{wild}/Ex3^{mut}	1	1	0	0	2
	Ex1^{mut}/Ex3^{mut}	1	1	1	2	5 (25%)
Lung complemented		1	1	1	2	5 (100%)

Table S3. Results of blastocyst complementation for lung generation at the adult stage. Related to Table 1.

		Exp1	Exp2	Exp3	Exp4	Exp5	Exp6	Exp7	Exp8	Total
Blastocysts injected		78	62	96	87	84	42	129	122	700
Blastocysts transferred		78	59	83	66	74	42	121	115	638
Fetuses(alive)		28(20)	6(3)	22(13)	18(15)	17(11)	16(12)	30(14)	16(8)	153(96)
Phenotype	Normal	23	6	19	17	17	14	24	14	134
	Limb defect	5	0	3	1	0	2	6	2	19
Genotype	Fgf10 $^{wild}/_{wild}$	9	4	10	4	12	3	13	6	61
	Ex1^{mut}/Ex3^{wild}	8	1	2	2	0	2	3	2	20
	Ex1^{wild}/Ex3^{mut}	4	0	5	2	2	6	5	4	28
	Ex1^{mut}/Ex3^{mut}	6	0	3	2	0	4	7	3	25
Chimeric fetuses		9	5	13	12	13	4	12	8	76
	Died	3	3	5	2	6	2	10	5	36
	Alive	6	2	8	10	7	2	2	3	40
Chimeras weaned		3	1	4	2	1	1	2	2	16
Lung complemented		1	0	0	1	0	1	1	1	5